NASA TN D-657

TECHNICAL NOTE

D-657

A THEORETICAL INVESTIGATION OF VORTEX-SHEET DEFORMATION BEHIND A HIGHLY LOADED WING AND ITS EFFECT ON LIFT

By Clarence D. Cone, Jr.

Langley Research Center
Langley Field, Va.

NATIONAL AERONAUTICS AND SPACE ADMINISTRATION
WASHINGTON
April 1961

NATIONAL AERONAUTICS AND SPACE ADMINISTRATION

TECHNICAL NOTE D-657

A THEORETICAL INVESTIGATION OF VORTEX-SHEET DEFORMATION BEHIND A HIGHLY LOADED WING AND ITS EFFECT ON LIFT[1]

By Clarence D. Cone, Jr.

SUMMARY

The induced drag polar is developed for wings capable of attaining extremely high loadings while possessing an elliptical distribution of circulation. This development is accomplished through a theoretical investigation of the vortex-wake deformation process and the deduction of the airfoil forces from the impulse and kinetic energy contents of the ultimate wake form. The investigation shows that the induced velocities of the wake limit the maximum lift coefficient to a value of 1.94 times the wing aspect ratio, for aspect ratios equal to or less than 6.5, and that the section properties of the airfoil limit the lift coefficient to 12.6 for aspect ratios greater than 6.5. Relations are developed for the rate of deformation of the vortex wake. It is also shown that linear wing theory is applicable up to lift coefficients equal to 1.1 times the aspect ratio.

INTRODUCTION

The development in recent years of advanced methods of boundary-layer control has made possible the attainment of very high lift coefficients with two-dimensional airfoil sections. Use of boundary-layer control on three-dimensional wings has likewise resulted in large increases in the maximum sectional circulations by preventing flow separation at high angles of attack. For a wing of finite span, however, this increased circulation is necessarily accompanied by an increasingly powerful trailing vortex system. The velocities induced in the vicinity of the wing by this system can become quite large, with a pronounced effect on the wing aerodynamic force, especially on the lift component. Successive increases in circulation produce diminishing increases in wing lift.

---

[1]The basic information presented herein was a part of a thesis entitled "The Limit of Circulation Lift on Airfoils of Finite Aspect Ratio" which was offered in partial fulfillment of the requirements for the degree of Master of Aeronautical Engineering, University of Virginia, Charlottesville, Virginia, May 1960. However, some additional material on the effects of wake deformation on longitudinal stability has been added.

From a design and performance standpoint it thus becomes of considerable importance to determine these wake effects in a quantitative manner. It is customary practice in conventional wing design to employ linear wing theory; this is justified since normal wing stall limits the maximum lift coefficient to relatively low values. For wings intended to operate at very high lift coefficients, however, the question arises as to the limit of the valid use of linear theory, since the linearizing assumptions are no longer justified for large deformations and displacements of the wake.

The present investigation has as its object, therefore, the quantitative estimation of the effects of the vortex wake deformation on the wing aerodynamic forces, with view to establishing the limiting lift coefficient for linear-theory application, and also the nature and magnitude of the deviation from the linear prediction at the higher lift coefficients. This development is accomplished by considering in some detail the rolling-up process of the wake and by deducing the aerodynamic forces from the impulse and kinetic energy of the final wake form. The results are presented in the form of the wing-induced drag polar, for all aspect ratios. As a corollary, for use in stability analyses, the rate of rollup of the vortex sheet is investigated and an expression is developed for the distance required for complete rollup, for a given lift coefficient and aspect ratio.

The basic analysis is carried out for the specific case of a conventional wing which maintains an elliptical distribution of circulation at all lift coefficients. The various wing-propulsion systems - such as the jet-flap wing - are excluded. The elliptical distribution is chosen because it yields results which are generally applicable to the more common planforms where the larger part of the vorticity is shed near the wing tips. The methods of the analysis are, however, general and may be applied to other distributions, although the calculations may be more involved.

Throughout the analysis the air is treated as an inviscid, incompressible fluid. Inasmuch as the attainment of high lift coefficients by actual wings requires the removal or reenergization of the boundary-layer air, the production of a large viscous wake by the airfoil is precluded and viscous effects are negligible. In the sequel, therefore, the wake referred to is the vortex wake associated with the wing circulation gradient and not a viscous wake.

SYMBOLS

A	aspect ratio, $\frac{b^2}{S_w}$
A'	cross-sectional area of the ovoid wake
a	circle radius (Joukowski transformation); ellipse major semiaxis
b	wing span; ellipse minor semiaxis
C_{Di}	induced drag coefficient, $\frac{D_i}{\frac{\rho V^2}{2} S_w}$
C_L	lift coefficient, $\frac{L}{\frac{\rho V^2}{2} S_w}$
c	wing chord
D_i	induced drag force
d	vortex sheet rollup distance (along X-axis)
$d\vec{S}$	vector element of surface area
$d\vec{s}$	vector element of arc length
E	total wake kinetic energy
E'	kinetic energy per unit length of subcore
$\vec{F}$	wing aerodynamic force vector
$\vec{F}'$	component of $\vec{F}$ due to momentum changes
F_R	resultant force on bound vortex system
I'	impulse per unit length of wake
$\vec{I}$	total wake impulse vector

J	vortex moment of inertia about system center of gravity
L	lift force
l	generalized length
M'	hydrodynamic mass per unit length of wake
n	number of turns per unit length of vortex helix
P	denotes specific point in space
$\vec{q}$	local velocity vector of induced field
q_o	velocity of center of gravity of generalized vortex system
R_1, R_2, r	radial distances from vortex core centers
r_o	radius of fully developed vortex core
r_1, r_2	normalized radial distances from vortex centers, $\frac{R_1}{b}$ and $\frac{R_2}{b}$, respectively
S	general surface area
S_w	wing area
t	time
U	general stream velocity
u	x-component of induced velocity
$V, \vec{V}$	free-stream velocity, (vector)
$\vec{V}_R$	resultant velocity at wing section
v	y-component of induced velocity
v_T	circumferential velocity
W	complex potential, $\phi + i\psi$
w	z-component of induced velocity

$\bar{w}$	velocity of center of gravity of vortex sheet
$\vec{x}$	unit vector along positive X-axis
$\bar{y}$	lateral coordinate of center of gravity of vortex system
z'	complex variable in Y-Z plane, $y + iz$
$\bar{z}$	vertical coordinate of center of gravity of vortex system
$\vec{z}$	unit vector along negative Z-axis
α	geometrical angle of attack
α_a	absolute angle of attack
Γ	circulation, $\oint^C \vec{q}.d\vec{s}$
Γ_o	circulation around median section of wing
δ	inclination angle of final wake
η	dummy variable of integration
θ	generalized wake inclination angle
κ	vortex strength, $\frac{\Gamma_o}{2\pi}$
ρ	fluid mass density
$\frac{\rho V^2}{2}$	dynamic pressure
Σ	the wake vortex sheet
τ	time required for complete rollup of vortex sheet
ϕ	velocity potential
φ	eccentric angle, $\cos^{-1}\frac{2y}{b}$
ψ	stream function
$\vec{\Omega}$	surface vorticity of vortex sheet

Subscripts:

c	property of vortex core
i	index number
S	property associated with wing surface
x,y,z	components along X-, Y-, and Z-axis, respectively
Σ	property associated with vortex sheet

Superscript:

P	reference point at which velocity is computed

THE WAKE-DEFORMATION PROCESS

Wake-Induction Effects

Induced-velocity effects.- Consider a wing in steady flight operating with an elliptical distribution of circulation

$$\Gamma(y) = \Gamma_o\sqrt{1 - \left(\frac{2y}{b}\right)^2} \tag{1}$$

Emanating from the trailing edge is a vortex sheet whose intensity immediately behind the trailing edge is

$$\frac{d\Gamma}{dy} = -\Gamma_o\left(\frac{2}{b}\right)^2 \frac{y}{\sqrt{1 - \left(\frac{2y}{b}\right)^2}} \tag{2}$$

This sheet may be considered a superposition of an infinite number of vortex filaments each of strength $\frac{d\Gamma}{dy}\,dy$ as shown in figure 1.

At any point P in the flow field the total velocity (relative to the fixed airfoil) is the sum of the free-stream velocity $\vec{V}$, the induced velocity $\vec{q}_S^{\,P}$ associated with the bound vorticity, and the induced velocity $\vec{q}_\Sigma^{\,P}$ due to the wake vorticity. Vectorially,

$$\vec{q}^{\,P} = \vec{V} + \frac{1}{4\pi} \iint^{S} \vec{\Omega}_S \times \frac{\vec{r}}{r^3}\, dS + \frac{1}{4\pi} \iint^{\Sigma} \vec{\Omega}_\Sigma \times \frac{\vec{r}}{r^3}\, dS \qquad (3)$$

This velocity field also applies to the vortex sheet and since the field is not, in general, uniform, the vortex sheet undergoes deformation as it passes downstream. Since the vorticity distribution of the wake determines the effective velocity field in the vicinity of the airfoil, by equation (3), this wake deformation is reflected as a change in the aerodynamic force vector acting on the wing. As is evident from equations (2) and (3), a large-span wing with small Γ_o (small angle of attack) will produce a relatively weak wake and the rate of deformation will be small; thus, the wake will maintain its sheet form for a considerable distance downstream.

High circulation effects.- If now the elliptical circulation loading form as given by equation (1) is maintained while Γ_o is increased, the wake will increase in intensity according to the Helmholtz law of vortex continuity. The large induced velocities associated with the high intensity cause a rapid deformation of the vortex sheet which, in addition to being displaced downward, begins to roll up from the edges. The downward progression of the wake causes it to be inclined to the free-stream-velocity direction by an angle $\theta = \theta(x)$. The rollup process causes the vorticity of the initial sheet to become increasingly concentrated into two vortex cores, and the resulting alteration of the induced field decreases the downward progression of the wake so that θ, in general, decreases in the downstream direction ($d\theta/dx$ negative). A generalized sketch of this variation of the wake angle is shown in figure 2. Here the angle θ is the inclination of the forming vortex cores. Far downstream, where the wake has reached a stable state of deformation (has become fully rolled up) the inclination angle is denoted by $\delta = \theta(\infty)$.

The wake deformation has two primary effects on the flow at the wing. First, the result of the inclination of the wake is that the velocity $\vec{q}_\Sigma^{\,P}$ induced at the airfoil is rotated forward as it increases in magnitude (fig. 3). Second, the concentration of the vorticity into cores causes a variation of the magnitude of the downwash across the span. Since the wake intensity increases with Γ_o so does the rate at which the sheet rolls up, and also, the angle of inclination of the wake increases. Thus, the downwash variation across the span becomes a function of Γ_o, for a wing of given span. For a wing with given Γ_o, as the span is decreased the intensity of the wake increases and additionally the wake becomes more narrow, so that the deformation will proceed

more rapidly for a low-aspect-ratio wing than for one with high aspect ratio. Thus, the form of the downwash distribution is also a function of aspect ratio.

The inclination of the wake introduces at the wing an induced-velocity component opposing the free-stream velocity $\vec{V}$; thus, the resultant effective velocity vector $\vec{V}_R$ existing at a section of the wing decreases in magnitude and is rotated downward as the section circulation is increased. Both of these effects lessen the increment in lift which accompanies the circulation increase.

In order to obtain an increase in circulation it is necessary to increase the absolute angle of attack α_a of the section with respect to $\vec{V}_R$. However, as the geometrical angle of attack of a section is increased the velocity $\vec{V}_R$ decreases in magnitude and rotates in a direction so as to reduce the absolute angle of attack; therefore, the variation of Γ with geometrical angle of attack becomes nonlinear in the high circulation range so that the slope $d\Gamma/d\alpha$ decreases. Also, since the resultant velocity varies across the span, $\vec{V}_R = \vec{V}_R(y)$, due to the wake deformation, and the form of this velocity variation varies with Γ_o, the nature of the variation of sectional lift with angle of attack becomes quite complex.

In the foregoing discussion the circulation distribution $\Gamma(y)$ has been specified as being elliptical. In order to maintain such a distribution physically, it would be necessary to carefully tailor the wing geometry so as to accommodate the resultant-velocity variation $\vec{V}_R(y)$. Since $\vec{V}_R(y)$ also varies with Γ_o, it is clear that the wing geometry must be variable if the elliptical circulation distribution is to be maintained. Conversely, if the wing geometry is fixed, the form of $\Gamma(y)$ must change with Γ_o. Of course, from this simple analysis no quantitative statements can be made about the nature or rapidity of the resultant-velocity variation.

For the elliptical circulation loading, the value of $\vec{V}_R$ is uniform across the span of an elliptical wing for small values of Γ_o. However, for large values of Γ_o or small aspect ratios the rapid rollup of the vortex sheet will tend to change the $\vec{V}_R$ distribution. Hence even though an elliptical distribution of circulation may exist on a wing the lift distribution, which is dependent on $\vec{V}_R$, may therefore be quite different in form.

The results of this simple qualitative analysis indicate that the wake effects will set a limit on the maximum lift coefficient of a finite-span wing. In order to obtain a quantitative estimate of these effects it is necessary to consider the details of the wake deformation.

Development of the Final Wake Form

Consider now a straight wing of any aspect ratio operating with the elliptical circulation loading of equation (1). It is prescribed that the loading shall remain elliptical at all values of lift coefficient. This condition may be physically realized by suitably varying the sectional camber of the wing for each value of C_L or by properly twisting the wing. The intensity of the trailing vortex sheet at the trailing edge is given by equation (2). The flat vortex sheet is an unstable form of vorticity and, for reasons to be discussed later, proceeds to roll in from the edges and to travel downward in the center so that relatively soon after its formation it appears somewhat as shown in figure 4. This rolling-up and displacement process continues until some distance downstream the original vortex sheet has separated in the middle and become coiled up into two cores of concentrated vorticity which are inclined by an angle δ to the free-stream flow. These approximately circular cores extend on downstream to infinity where they join the ends of the starting vortex.

If now the form and properties of the final wake can be quantitatively determined, the aerodynamic force on the wing can be determined by suitable application of the general energy and momentum theorems. In order to establish the final wake form the system of reference axes shown in figure 5 is used, where the origin is located at the midspan of the trailing edge and the X-axis is parallel to the cores of the final wake, which is inclined to the free-stream velocity by the angle δ. The axes move with the airfoil so that the flow is steady. The positive directions of the induced-velocity components u, v, and w are as indicated. (The components of V are $V \cos \delta$ and $V \sin \delta$ in the x- and z-direction, respectively (fig. 6).)

Under the action of the total velocity field the vortex filaments comprising the initial vortex sheet assume a helical form as they wind about the growing cores (fig. 4). Far downstream where the rolling up may be considered complete, this system of helical filaments approximates what might be called a pair of vortex solenoids. These fluid solenoids possess the same induction properties as their electrical counterparts, with proper accounting, of course, for the fluidity of the cores. Far downstream the flow inside the cores has the components $V \cos \delta + u$, v, and $w - V \sin \delta$, while outside the cores it has the velocity components $V \cos \delta$, v, and $w - V \sin \delta$ in the x-, y-, and z-direction, respectively.

Considering now a narrow strip of the flat vortex sheet taken near the trailing edge of the wing (as in fig. 4), if the rate of deformation of the sheet in the longitudinal direction is small, the wake may be established to a good approximation by considering the rolling up as a two-dimensional process and tracing the deformation of the two-dimensional strip as it moves downstream. At the higher deformation rates the assumption of a two-dimensional rollup appears less accurate since the shape of the wake on either side of the strip will vary somewhat from that of the strip. However, the assumption is made that up to the maximum lift of the airfoil the rate of deformation is sufficiently low so that the two-dimensional deformation may be used to construct a first-order approximation of the wake form. A justification of this assumption lies in the fact that the primary concern is not with an accurate description of the entire sheet deformation but with only the relatively small region where the sheet is adding to the core. With this assumption the cross section of the wake at any distance downstream is that of the deformed two-dimensional strip.

Properties of two-dimensional vortex systems.- The following two theorems which will be of subsequent use are derived in detail in reference 1:

Theorem 1: If a system of two-dimensional vortices exists on one side of a flat bounding wall the center of gravity of the vortex system will translate parallel to the wall with the velocity

$$q_o = \frac{\sum \Gamma_i q_i}{\sum \Gamma_i} = \frac{F_R}{\rho \sum \Gamma_i} \tag{4}$$

where Γ_i indicates the circulation of the individual vortices and F_R is the magnitude of the force exerted by the fluid on the bounding wall. The center of gravity of a vortex system is obtained from the relations

$$\left.\begin{aligned} \bar{y} &= \frac{\sum y_i \Gamma_i}{\sum \Gamma_i} \\ \bar{z} &= \frac{\sum z_i \Gamma_i}{\sum \Gamma_i} \end{aligned}\right\} \tag{5}$$

for a y,z coordinate system.

Theorem 2: If a vortex system produces no moment with respect to its center of gravity the moment of inertia of the system will remain constant in value for all time,

$$\sum \Gamma_i r_i^2 = \text{Constant} \tag{6}$$

Here r_i is the distance of the vortex Γ_i from the system center of gravity.

These theorems are written for a system of discrete vortices. For the case where the system is continuous (i.e, a vortex sheet), the summation $\sum$ is replaced by a line integration along the sheet.

Deformation of the wake strip.- These results may now be applied to determine the deformation of the initially flat strip of wake taken from the vortex sheet immediately behind the trailing edge. A y,z coordinate system as shown in figure 7 is used in which the vortex strip initially lies along the Y-axis with the origin located at the center of the strip. Since the two halves of the strip are mirror images, the plane $y = 0$ may be taken as a solid boundary and only the half $0 \leqq y \leqq \frac{b}{2}$ need be considered.

The intensity of the strip is initially

$$\frac{d\Gamma}{dy} = -\Gamma_o \left(\frac{2}{b}\right)^2 y \left[1 - \left(\frac{2y}{b}\right)^2\right]^{-1/2}$$

and the center of gravity of the strip is

$$\left.\begin{aligned} \bar{y} &= \frac{\int_0^{b/2} y \frac{d\Gamma}{dy}\, dy}{\int_0^{b/2} \frac{d\Gamma}{dy}\, dy} = \frac{\pi b}{8} \\ \bar{z} &= 0 \end{aligned}\right\} \tag{7}$$

The strip will initially tend to move downward as a flat sheet with a velocity given by $w = \frac{\Gamma_o}{2b}$. However, a flat vortex sheet is inherently unstable and begins to curl up at the edges as it travels downward. This instability may be physically explained in the following qualitative manner. The flow field about the flat sheet is identical to that about a translating plate where very low pressures occur at the edges due to the very high velocities. The fluid sheet is unable to resist these suction pressures at the edges and under the pressure gradient, rotational fluid from the interior flows into the tip region thereby increasing the circulation about the tip. (The vortex "sheet," it should be noted, is the idealized form for a finite thickness layer of rotational fluid.) The initial vorticity distribution is thus altered and the velocity field produced is such that it causes the sheet to begin winding about the tip core. The rolling-up process during the very first moments of deformation have been treated in detail by Kaden (ref. 2). A numerical investigation of the rolling-up process using a row of discrete vortices to represent the vortex sheet has also been performed by Westwater (ref. 3). Both of these (two-dimensional) treatments indicate that the semisheet $\left(0 \leq y \leq \frac{b}{2}\right)$ coils up into a spiral of the form shown in figure 8.

As the strip rolls up and moves downward its center of gravity moves along the line $y = \frac{\pi}{8}b$, as predicted by theorem 1. The initial velocity of the center of gravity is $\bar{w} = \frac{\Gamma_o}{2b}$ and after rollup is complete the velocity is $\bar{w} = 2\frac{\Gamma_o}{\pi^2 b}$.

Considering again the initially flat strip of figure 7, the total circulation associated with a segment $y_1 \leq y \leq \frac{b}{2}$, using equation (2), is

$$\Gamma(y_1) = \int_{y_1}^{b/2} \frac{d\Gamma}{dy}\, dy = \Gamma_o \sqrt{1 - \left(\frac{2y_1}{b}\right)^2} \tag{8}$$

For convenience in subsequent derivations, y is now written in terms of the eccentric angle φ,

$$y = \frac{b}{2}\cos\varphi \tag{9}$$

Then,

$$\frac{d\Gamma}{dy} = -\Gamma_o \frac{2}{b} \cot \varphi \tag{10}$$

$$\Gamma(y_1) = \Gamma_o \sin \varphi_1 \tag{11}$$

The center of gravity of the segment $y_1 \leqq y \leqq \frac{b}{2}$ is

$$\left.\begin{aligned} \bar{y}_1 &= \frac{1}{\Gamma(y_1)} \int_{b/2}^{y_1} y \frac{d\Gamma}{dy} dy = \frac{b}{4 \sin \varphi_1}\left(\varphi_1 + \frac{1}{2} \sin 2\varphi_1\right) \\ \bar{z}_1 &= 0 \end{aligned}\right\} \tag{12}$$

With respect to the origin $y = 0$, the moment of inertia of this segment is

$$J_o(y_1) = \int_{y_1}^{b/2} y^2 \frac{d\Gamma}{dy} dy = \Gamma_o\left(\frac{b}{2}\right)^2 \sin \varphi_1 \left(1 - \frac{1}{3} \sin^2 \varphi_1\right) \tag{13}$$

Transferring this moment of inertia to the center of gravity of the segment $y_1 \leqq y \leqq \frac{b}{2}$ gives

$$\begin{aligned} J(y_1) &= J_o(y_1) - \Gamma(y_1)\bar{y}_1^2 \\ &= \Gamma_o\left[\left(\frac{b}{2}\right)^2 \sin \varphi_1 \left(1 - \frac{1}{3} \sin^2 \varphi_1\right) - \left(\frac{b}{4}\right)^2 \frac{1}{\sin \varphi_1}\left(\varphi_1 + \frac{1}{2} \sin 2\varphi_1\right)^2\right] \end{aligned} \tag{14}$$

Now as the rollup proceeds, the strip coils up in a nearly circular form, as shown by the results of Kaden (ref. 2) and Westwater (ref. 3); therefore, the segment $y_1 \leqq y \leqq \frac{b}{2}$ coils into a spiral contained within a circle of radius r_1. As the circular core grows, the circulation of the enclosed vorticity is given by

$$\Gamma(r_1) = \Gamma(y_1) \tag{15}$$

Similarly the moment of inertia of the segment after coiling is equal to its original value by theorem 2,

$$J(r_1) = J(y_1) \tag{16}$$

Thus when r increases by dr, y must decrease by dy (whence φ increases by $d\varphi$) and the corresponding increments in core circulation and moment of inertia become

$$\frac{d\Gamma}{dr}\,dr = \frac{d\Gamma}{d\varphi}\,d\varphi = \Gamma_o \cos\varphi\, d\varphi \tag{17}$$

$$\frac{d\Gamma}{dr}\,r^2 dr = \frac{dJ}{d\varphi}\,d\varphi \tag{18}$$

Differentiating equation (14) gives

$$\frac{dJ}{d\varphi} = \Gamma_o\left(\frac{b}{2}\right)^2\left[\cos^3\varphi + \frac{\cos\varphi}{4\sin^2\varphi}\left(\varphi + \frac{1}{2}\sin 2\varphi\right)^2 - \frac{1}{2\sin\varphi}\left(\varphi + \frac{1}{2}\sin 2\varphi\right)(1 + \cos 2\varphi)\right] \tag{19}$$

Substitution of equations (17) and (19) into equation (18) yields

$$\frac{4r^2}{b^2} = \cos^2\varphi + \frac{1}{4\sin^2\varphi}\left(\varphi + \frac{1}{2}\sin 2\varphi\right)^2 - \frac{\cos\varphi}{\sin\varphi}\left(\varphi + \frac{1}{2}\sin 2\varphi\right) \tag{20}$$

Since φ and y are related by the expression $\cos\varphi = \frac{2}{b}y$, equation (20) denotes the relation between y and r. A plot of $\frac{2y}{b}$ against $\frac{2r}{b}$ as given by equation (20) is shown in figure 9. For small values of φ ($\varphi \to 0$) equation (20) can be linearized by a limiting process to give

$$\frac{2r}{b} = \frac{2}{3}\sin^2\varphi \tag{21}$$

or in terms of y $\left(y \rightarrow \frac{b}{2}\right)$, this becomes after a similar limiting process

$$r = \frac{2}{3}\left(\frac{b}{2} - y\right) \tag{22}$$

A small segment of the strip near the tip is thus coiled within a circle of radius equal to 2/3 the length of the segment. Equation (22) has been plotted in figure 9 where it is seen that it closely approximates equation (20) through most of the range. Hence equation (22) may, with sufficient accuracy, be used to obtain the final core properties since over 95 percent of the total vorticity is contained within the core region where the agreement is quite good. Also shown in figure 9 is a plot of $\frac{\Gamma}{\Gamma_o}$ against $\frac{2r}{b}$. Figure 9 is taken from the results of reference 1.

These results lead to the picture of two final vortex cores of radius $r_o = \frac{b}{3}$ spaced a distance $\frac{\pi b}{4}$ apart with the vorticity heavily concentrated near the centers, as shown in figure 10.

Final wake form.- The deformation of the vortex strip is now traced as it passes downstream by using the axis system of figure 5 with the assumption that the deformation follows the relations just established. Everywhere outside the developing cores the x-component of velocity is taken to be $V \cos \delta$, while the y- and z-components are v and $w - V \sin \delta$, respectively. When the core has grown to a radius r the circulation of the enclosed vorticity is $\Gamma(r)$. Since the cores are nearly circular in form, especially for small values of r, the tangential velocity v_T at the core surface $\left(v_T = \sqrt{v^2 + (w - V \sin \delta)^2}\right)$ is assumed uniform and is therefore obtainable from the circulation,

$$v_T(r) = \frac{\Gamma(r)}{2\pi r} \tag{23}$$

The core grows by the addition of vortex filaments from the sheet to its outer surface. The filaments add along the streamlines which are determined by the velocity components $V \cos \delta$ and v_T to form concentric vortex helices of intensity $\frac{d\Gamma}{dr}$. (See fig. 11.) This winding process continues until the original sheet has been consumed.

By use of equation (22) relating the core properties to those of the initial sheet, the circulation, intensity, and tangential velocity

distributions within the fully developed cores can be determined as pure functions of the radius. The core circulation is

$$\Gamma(r) = \Gamma_o\left[1 - \frac{1}{b^2}(b - 3r)^2\right]^{1/2} \tag{24}$$

the intensity is

$$\frac{d\Gamma}{dr} = \Gamma_o \frac{3}{b^2}(b - 3r)\left[1 - \frac{1}{b^2}(b - 3r)^2\right]^{-1/2} \tag{25}$$

and, by using equation (23), the tangential velocity is

$$v_T = \frac{\Gamma_o}{2\pi r}\left[1 - \frac{1}{b^2}(b - 3r)^2\right]^{1/2} \tag{26}$$

It is evident from equations (25) and (26) that both $\frac{d\Gamma}{dr}$ and v_T become infinite at $r = 0$. These are also properties of a mathematical point vortex. Unlike the point vortex, however, the velocity distribution given by equation (26) leads to a finite kinetic energy for the core flow, as will be shown later.

Axial velocity field $u(r)$.- The preceding development led to the picture of the cores as a superposition of concentric vortex helices, each helix being a vortex filament from the original sheet. A helix of radius r has an intensity $\frac{d\Gamma}{dr}$ and induces a constant longitudinal velocity du across its interior. As shown in appendix A the differential induced velocity due to this elemental helix is

$$du = n(r)\frac{d\Gamma}{dr}\,dr \tag{27}$$

where $n(r)$ is the number of vortex turns per unit length of the core and

$$n(r) = \frac{v_T(r)}{2\pi r\left[V\cos\delta + u(r)\right]} \tag{28}$$

At the surface of the developing core the longitudinal velocity is V cos δ, since u = 0; therefore, n(r) is given by

$$n(r) = \frac{v_T(r)}{2\pi r V \cos \delta}$$

However, as more vortex lines are added, the longitudinal velocity u(r) within the core tends to change, thus changing n(r) of the filaments within the core. After the cores are fully developed, n(r) is given by equation (28). The value of u at a given radius is obtained by summing the velocities induced by the helices exterior to that radius,

$$u(r) = \int_r^{b/3} n(\eta) \frac{d\Gamma}{d\eta} d\eta \tag{29}$$

where η denotes a dummy variable of integration. For the region $\frac{b}{3} \geq r \geq 0$, using equations (26) and (28) gives

$$n(r) = \frac{\Gamma_o}{(2\pi r)^2 \left[V \cos \delta + u(r)\right]} \left[1 - \frac{1}{b^2}(b - 3r)^2\right]^{1/2} \tag{30}$$

therefore,

$$u(r) = \frac{3}{4\pi^2 b^2} \Gamma_o^2 \int_r^{b/3} \frac{1}{\left[V \cos \delta + u(\eta)\right]} \left(\frac{b}{\eta^2} - \frac{3}{\eta}\right) d\eta \tag{31}$$

This integral equation has the equivalent differential form

$$(V \cos \delta + u) \frac{du}{dr} = \frac{3\Gamma_o^2}{4\pi^2 b^2} \left(\frac{b}{r^2} - \frac{3}{r}\right)$$

The solution of this equation, subject to the condition $u\left(\frac{b}{3}\right) = 0$, gives the axial velocity field. Although the differential equation is non-linear, it is readily integrated after separating the variables. Thus,

$$\int_0^u (V \cos \delta + u')du' = \frac{3\Gamma_o^2}{4\pi^2 b^2} \int_r^{b/3} \left(\frac{b}{\eta^2} - \frac{3}{\eta}\right) d\eta$$

Expansion of this equation yields

$$\frac{1}{2}u^2 + uV\cos\delta = \frac{9\Gamma_o^2}{4\pi^2 b^2}\left[\log_e r - \log_e\frac{b}{3} + \frac{b}{3r} - 1\right]$$

and since

$$\frac{\Gamma_o^2}{b^2} = \frac{\pi^4}{4}V^2(1 - \cos^2\delta)$$

the axial velocity field becomes, as a function of core radius and wake inclination angle,

$$u = \sqrt{V^2\cos^2\delta + \frac{9\pi^2}{8}V^2(1 - \cos^2\delta)\left(\frac{b}{3r} - 1 - \log_e\frac{b}{3r}\right)} - V\cos\delta \qquad (32)$$

or

$$u = V\cos\delta\left[\sqrt{1 + \frac{9\pi^2}{8}(\sec^2\delta - 1)f_1(r)} - 1\right] \qquad (33)$$

where

$$f_1(r) = \left(\frac{b}{3r} - 1 - \log_e\frac{b}{3r}\right)$$

This relation (eq. (32)) predicts an infinite value for u at $r = 0$, but unlike the velocity field v_T, the kinetic energy of the $u(r)$ field is infinite. In order to obtain a more useful picture of the axial velocity field, divide both sides of equation (33) by $V\cos\delta$ to obtain

$$\frac{u}{V\cos\delta} = \sqrt{1 + \frac{9\pi^2}{8}(\tan^2\delta)f_1(r)} - 1 \qquad (34)$$

which gives the ratio of the axial velocity u to the wake-direction component of the free-stream velocity. A plot of $f_1(r)$ against r/b is presented in figure 12. Now for small values of δ, say $\delta = 5^\circ$, $\tan^2\delta = 0.008$. For most of the core area, say $r = 0.1b$ (this includes 91 percent of the total core area), $f_1(r)$ is small, reaching the value of 1.1 at $r = 0.1b$. Thus for small wake angles the axial velocity u is of negligible magnitude over most of the core area. Very near the center, however, the ratio attains very large values, becoming infinite

at the core centers, even for values of δ approaching 0. It is obvious from physical considerations that the large core velocities cannot exist, and the reason for their prediction by equation (34) can be directly traced to the assumptions made in the derivation of this result.

In the derivation of equation (29) (see appendix A), it was assumed that n was sufficiently great that each vortex turn could be considered to lie in a plane. This assumption is equivalent to a pitch approaching zero for all helices. However, an analysis of equation (30) with $u = 0$ shows that even for appreciable values of δ ($\delta \leq 30^\circ$), n is small ($n \ll 1$) for the outer helices (r near $b/3$). Hence, the planar condition is not approached and due to the inclination of the induced-velocity vector with respect to the core axis the potential magnitude of the axial velocity over the core interior will not be realized. Additionally, these same effects on interior helices may produce negative axial velocities which can counteract the positive induced velocities of the outer helices.

In the derivation of equation (26) the rollup of an infinitely thin vortex sheet was considered, so that the vorticity at the tips $\left(y = \pm\frac{b}{2}\right)$ was infinite. In reality, the vortex-sheet wake consists of a layer of rotational fluid which attains appreciable thickness near the tip (ref. 4 and fig. 13). Since the vorticity of the layer is spread over a finite volume of fluid the vorticity density at the tip cannot be infinite, for a finite circulation in a circuit surrounding the tip region. Surveys show that near the center of the rolled-up vortex cores the fluid possesses a large but constant vorticity and the fluid there must rotate as a solid. Within this small subcore, $v_T \to 0$ as $r \to 0$, so that n again becomes increasingly smaller as the center is approached. Thus, no infinite axial velocities can actually occur.

These effects associated with a more accurate representation of the physical flow regime as it actually exists, offer a sufficient explanation as to the invalidity of equation (34) very near the core centers.

It is of course possible to extend the analysis to a more refined consideration of the physical flow regime so as to include the effects of the subcore on the axial velocity field. The primary problem then is to establish the size of the subcores. However, due to the complexity of such a treatment, and in view of the fact that u is very small, even for relatively large values of δ ($\delta \leq 30^\circ$), as is confirmed by experimental evidence (ref. 4), such an analysis is not justified for the purposes of the present investigation. Therefore,

it is now assumed, to the degree of accuracy of the foregoing assumptions, that the axial velocity field is sufficiently small so that its effects may be neglected in the calculation of the airfoil forces.

Rate of Deformation of the Vortex Sheet

The preceding results concerning the deformation of the vortex sheet can be used to determine the degree to which the sheet has rolled up at any given downstream station ("downstream" referring to distance along the X-axis in fig. 5). Considering a cross section through a developing core, such as shown in figure 14 where v_T is the tangential velocity at the core surface (assumed uniform around the periphery), the rate at which the sheet adds to the core is given by

$$\frac{dy}{dt} = v_T \tag{35}$$

where dy is an elemental length of the sheet. The relation between y and r as previously developed is (eq. (22))

$$y = \frac{3}{2}\left(\frac{b}{3} - r\right)$$

whence

$$dy = -\frac{3}{2}\,dr \tag{36}$$

The time required for the core to develop to a radius r is therefore

$$t = \int_0^r \frac{3}{2}\frac{d\eta}{v_T(\eta)}$$

Substitution of v_T from equation (26) yields

$$t = \frac{6}{\pi V b \sin\delta}\int_0^r \eta\left[1 - \frac{1}{b^2}(b - 3\eta)^2\right]^{-1/2} d\eta \tag{37}$$

The downstream distance x corresponding to this time is

$$x = Vt\cos\delta = \frac{6}{\pi b}\cot\delta\int_0^r \eta\left[1 - \frac{1}{b^2}(b - 3\eta)^2\right]^{-1/2} d\eta \tag{38}$$

The rolling-up process is complete when $r = \frac{b}{3}$, and the time and distance for complete development are obtained by setting the upper limit equal to $b/3$ in the common integral of equations (37) and (38).

Using the general result

$$\int \frac{p^2}{(a^2 - p^2)^{1/2}}\, dp = -\frac{p}{2}\sqrt{a^2 - p^2} + \frac{a^2}{2}\sin^{-1}\frac{p}{a} + \text{Constant}$$

and associating p with η $\left(p = \eta^{1/2}\right)$, the common integral of equations (37) and (38) can be evaluated to yield the results

$$t = \frac{4b}{\pi V \sin\delta}\left[-\frac{1}{2}\sqrt{\frac{r}{b}}\sqrt{\frac{2}{3} - \frac{r}{b}} + \frac{1}{3}\sin^{-1}\sqrt{\frac{3}{2}\frac{r}{b}}\right] \tag{39}$$

$$x = \frac{4b}{\pi}\cot\delta\left[-\frac{1}{2}\sqrt{\frac{r}{b}}\sqrt{\frac{2}{3} - \frac{r}{b}} + \frac{1}{3}\sin^{-1}\sqrt{\frac{3}{2}\frac{r}{b}}\right] \tag{40}$$

for any value of r.

For complete rollup of the elliptical sheet, $r = \frac{b}{3}$, therefore,

$$\tau = 0.1211\,\frac{b}{V}\cos\delta \tag{41}$$

$$d = 0.1211b\cot\delta \tag{42}$$

For small angles,

$$\delta = \frac{2}{\pi^2}\frac{\Gamma_o}{Vb}$$

Since for an elliptical wing

$$\delta = \frac{4}{\pi^3}\frac{C_L}{A}$$

equations (41) and (42) may be written in the following form:

$$\tau = 0.93\,\frac{b}{V}\frac{A}{C_L} \tag{43}$$

$$d = 0.93b \frac{A}{C_L} \tag{44}$$

This form is useful for comparison with Kaden's results (ref. 2).

DETERMINATION OF THE AERODYNAMIC FORCES

The lifting airfoil experiences a resultant aerodynamic force $\vec{F}$ which is composed of the lift and induced drag components taken normal and parallel, respectively, to the free-stream velocity. In the present system of axes (fig. 5) the aerodynamic force $\vec{F}$ is resolved into components F_z and F_x as shown in figure 15 where the positive force directions are indicated by the vectors. The transformation equations for the two force systems are, from figure 15,

$$L = F_z \cos \delta - F_x \sin \delta \tag{45}$$

$$D_i = F_z \sin \delta + F_x \cos \delta \tag{46}$$

Determination of any two force components allows the calculation of the resultant aerodynamic force $\vec{F}$; therefore, F_z and D_i will be determined for this purpose.

Determination of F_z

Far behind the airfoil the wake consists of two vortex cores containing the coiled vortex sheet. Within the vortex cores the motion is irrotational except for the surface of velocity discontinuity representing the coiled sheet. This wake has been created from air which was initially at rest (considering the flight of the wing through still air). The creation of the motion associated with a unit length of the wake has required the application of a definite vector impulse $-\vec{I}'$ by the airfoil. From the viewpoint of a stationary airfoil in a free-stream flow of velocity $\vec{V}$ (steady flow), the instantaneous time rate of change of the total impulse of the wake is constant and equal to a component of the aerodynamic force acting on the control volume,

$$\vec{F}' = \frac{d\vec{I}}{dt} \tag{47}$$

Since the impulse is a vector quantity, it may be resolved into its components, whence

$$\left.\begin{aligned} F_z' &= \frac{dI_z}{dt} \\ F_x' &= \frac{dI_x}{dt} \\ F_y' &= 0 \end{aligned}\right\} \qquad (48)$$

$\left(F_y' = 0 \text{ because of the plane of symmetry of the wake}\right)$.

The coiled vortex sheet may be considered, as previously mentioned, as being formed from a superposition of concentric helical vortex filaments of strength $\frac{d\Gamma}{dr}\,dr$. Corresponding filaments (one from each core) form a vortex pair which may be considered part of the boundary of an infinite vortex ring of which the bounding filament is helical in form. The total impulse of a unit length of the wake may therefore be obtained by summing the impulse contributions of all the vortex filaments comprising the cores.

For any vortex ring formed by a closed vortex filament of strength Γ the impulse acting on the boundary generating the motion from rest is

$$\vec{I} = \iint^{S} \rho(\phi_a - \phi_b)\,d\vec{S} \qquad (49)$$

where $\rho\phi$ is the impulsive pressure acting at a point on a surface S having the ring as its boundary, and ϕ_a and ϕ_b refer to the potential values at neighboring points on either side of the surface (fig. 16). On passing through the surface the potential must suffer a jump equal to Γ whence $\phi_a - \phi_b = \Gamma$, and

$$\vec{I} = \iint^{S} \rho\Gamma\vec{n}\,dS \qquad (50)$$

where $\vec{n}\,dS = d\vec{S}$, gives the resultant linear impulse to generate the ring. The value of $\vec{I}$ is independent of the form of the surface S

taken, by applying Stokes' theorem. Since Γ is constant by Kelvin's circulation theorem $\left(\frac{D}{Dt}\right)\oint \vec{q}.d\vec{r} = 0$, the force required to increase the impulse of the ring is

$$\frac{d\vec{I}}{dt} = \rho\Gamma \frac{d}{dt} \iint^{S} \vec{n}\, dS \tag{51}$$

The impulse of a helical vortex pair located at radius r within the core is now determined. The axes of the helices are spaced $\pi b/4$ apart as shown in figure 17. Corresponding points on the two filaments may be connected by a straight line parallel to the Y-axis so that a surface may be constructed, all of whose generators are normal to the X- and Z-axes and connect corresponding points on the two helices as shown in figure 18. If this area is denoted by S, the impulse per unit length of the pair is

$$d\vec{I}' = \iint^{S} \rho \frac{d\Gamma}{dr} dr\vec{n}\, dS \tag{52}$$

The z-component of this impulse is

$$dI_z' = \rho \frac{d\Gamma}{dr} dr \iint^{S} \vec{n}.\vec{z}\, dS \tag{53}$$

where $\vec{z}$ is a unit vector parallel to the Z-axis. However $\vec{n}.\vec{z}\, dS$ is merely the projection of the area $\vec{n}\, dS$ on the X-Y plane (fig. 19), so that equation (53) becomes, considering the symmetry of the projection of a helix with regard to its axis,

$$dI_z' = \rho \frac{\pi}{4} b \frac{d\Gamma}{dr} dr \tag{54}$$

and this gives the z-impulse per unit length of a helical-filament pair.

From the results of the section "Axial velocity field u(r)," the longitudinal velocity u is negligible so that integration of equation (54) yields the simple result

$$F_z' = F_z = \int_0^{b/3} \rho \frac{\pi b}{4} V \cos\delta \frac{d\Gamma}{dr} dr = \rho \frac{\pi b}{4} \Gamma_o V \cos\delta \tag{55}$$

for the z-component of the aerodynamic force. This is exactly the same result as would be obtained by considering the cores as line vortices of strength Γ_o.

From figure 18 it is evident that there should exist also a force component F_x', since from the geometry of the wavy impulse surface it can be seen that

$$\iint^S \vec{x}.\vec{n}\, dS < 0$$

where $\vec{x}$ is a unit vector in the positive x-direction; that is, there is a net component of impulse surface area in the negative x-direction. This force F_x' is clearly the force associated with the increase in longitudinal momentum due to u. Under the assumption that u is negligible, $F_x' = 0$.

A second method for determining F_z through a consideration of the hydrodynamic mass of the wake body is given in appendix B. The results, as may be expected, are again identical to those for a vortex pair.

Determination of D_i

The component D_i of the aerodynamic force is determined by an integration of the wake kinetic energy. The basic relation for this calculation is the power equation,

$$\frac{dK}{dt} = VD_i = \rho V \cos\delta \iint^{\infty,0} \frac{v^2 + w^2}{2}\, dS + \rho V \cos\delta \iint^{S_c} \frac{u^2 + v^2 + w^2}{2}\, dS$$

$$+ \rho \iint^{S_c} \frac{u^2 + v^2 + w^2}{2}\, u\, dS \qquad (56)$$

where $\infty,0$ denotes an integration over a plane taken perpendicular to the cores and far downstream of the wing, of the area external to the vortex cores, and S_c denotes integration over the core areas. If u is considered negligible, equation (56) becomes simply,

(a) (b)

$$D_i = \rho \cos \delta \iint^{\infty,0} \frac{v^2 + w^2}{2} dS + \rho \cos \delta \iint^{S_c} \frac{v^2 + w^2}{2} dS \quad (57)$$

These integrals are designated (a) and (b) as shown.

Integral (a) is simply evaluated by considering the two-dimensional velocity field due to the vortex pair. The complex potential is (fig. 20)

$$W = i\kappa \log_e R_1 - i\kappa \log_e R_2 \quad (58)$$

where $\kappa = \frac{\Gamma_o}{2\pi}$. The stream function of the motion is $\psi = \kappa \log_e \frac{R_1}{R_2}$, so that

$$\frac{\rho}{2} \cos \delta \iint^{\infty,0} (v^2 + w^2) dS = \frac{\rho}{2} \cos \iint^{\infty,0} \left(w \frac{\partial \psi}{\partial y} - v \frac{\partial \psi}{\partial z} \right) dy\, dz$$

$$= \frac{\rho}{2} \cos \delta \iint^{\infty,0} \left[\frac{\partial}{\partial y} (w\psi) - \frac{\partial}{\partial z} (v\psi) \right] dy\, dz \quad (59)$$

since the flow is everywhere irrotational. By Stokes' theorem and equation (59)

$$\frac{\rho}{2} \cos \delta \iint^{\infty,0} (v^2 + w^2) dS = \frac{\rho}{2} \cos \delta \oint^{C} \psi (v\, dy + w\, dz) \quad (60)$$

where the contour C denotes the core boundaries and the connecting line as shown in figure 20. The integration is carried out in the positive direction with the enclosed area to the left. Since $(v\, dy + w\, dz) = v_T\, ds$, where v_T is the tangential speed at the core boundary, equation (60) becomes

$$\frac{\rho}{2} \cos \delta \iint^{\infty,0} (v^2 + w^2) dS = -\rho \cos \delta \oint^{C_1} \kappa v_T \log_e \frac{R_1}{R_2} ds \quad (61)$$

where C_1 denotes counterclockwise integration around the right core only. On this boundary $R_1 = \frac{b}{3}$ so that

$$-\oint^{C_1} \kappa v_T \log_e r_1 \, ds = -\frac{\Gamma_o^2}{2\pi} \log_e \frac{1}{3} \tag{62}$$

(In the expression $\log_e \frac{R_1}{R_2} = \log_e \frac{r_1 b}{r_2 b}$, b is cancelled before integration.) For r_2 we have

$$\oint^{C_1} \kappa(\log_e r_2) v_T \, ds = \frac{b}{3} \int_0^{2\pi} v_T \frac{\Gamma_o}{2\pi} \log_e r_2(\theta) d\theta \tag{63}$$

From the geometrical relationships of figure 21, the following functions of θ are obtained:

$$\left.\begin{aligned} v_T(\theta) &= \frac{\Gamma_o}{2\pi b}\left\{3 - \frac{1}{r_2(\theta)} \cos\left[\theta - \sin^{-1}\left(\frac{\sin\theta}{3r_2(\theta)}\right)\right]\right\} \\ r_2(\theta) &= \left[\left(\frac{\pi}{4} + \frac{1}{3}\cos\theta\right)^2 + \left(\frac{\sin\theta}{3}\right)^2\right]^{1/2} \end{aligned}\right\} \tag{64}$$

Graphical integration of equation (63) then yields

$$\oint^{C_1} \kappa(\log_e r_2) v_T \, ds = -6.432 \frac{\Gamma_o^2}{12\pi^2} \tag{65}$$

and integral (a) of equation (57) becomes

$$\frac{\rho}{2} \cos\delta \iint^{\infty,0} (v^2 + w^2) dS = 0.1205\rho \cos\delta \, \Gamma_o^2 \tag{66}$$

Integral (b) of equation (57) is to be evaluated over both vortex cores. If the geometrical relations of figure 22 are used, the core velocity components are

$$\left.\begin{aligned} v &= \frac{\Gamma_o}{2\pi}\left[\frac{r\sin\theta}{\left(\frac{\pi}{4}b + r\cos\theta\right)^2 + (r\sin\theta)^2} - \frac{\sin\theta}{r}\sqrt{1 - \frac{1}{b^2}(b - 3r)^2}\right] \\ w &= \frac{\Gamma_o}{2\pi}\left[\frac{\frac{\pi}{4}b + r\cos\theta}{\left(\frac{\pi}{4}b + r\cos\theta\right)^2 + (r\sin\theta)^2} - \frac{\cos\theta}{r}\sqrt{1 - \frac{1}{b^2}(b - 3r)^2}\right] \end{aligned}\right\} \quad (67)$$

The velocity v_T within the cores, as given by equation (26), becomes infinite at $r = 0$. The kinetic energy of the core however approaches a finite value. If a very small region near the center of the core where v_T becomes large is considered, the kinetic energy of this region can be obtained by summing the rotational and the translational energies. Thus,

$$dE' = \left(\frac{1}{2}\rho v_T^2 2\pi r\, dr + V^2\sin^2\delta\, \frac{1}{2}\rho 2\pi r\, dr\right)$$

where

$$v_T^2 = \frac{\Gamma_o^2}{4\pi^2}\frac{1}{r^2}\left[1 - \frac{1}{b^2}(b - 3r)^2\right]$$

and

$$\begin{aligned} E' &= \left\{\frac{\rho\Gamma_o^2}{4\pi}\int_0^r \frac{1}{\eta}\left[1 - \frac{1}{b^2}(b - 3\eta)^2\right]d\eta + \frac{2}{\pi^3}\frac{r^2}{b^2}\rho\Gamma_o^2\right\} \\ &= \left[\frac{1}{4\pi}\left(6\frac{r}{b} - \frac{9}{2}\frac{r^2}{b^2}\right) + \frac{2}{\pi^3}\frac{r^2}{b^2}\right]\rho\Gamma_o^2 \end{aligned} \quad (68)$$

and the kinetic energy per unit length of the core is finite, even though the rotational velocity is infinite at $r = 0$.

Now arbitrarily choosing a small value for r, say $r = 0.001b$, integral (b) can be evaluated by using equation (68) to obtain the induced drag corresponding to the energy in the region $0 \leq r \leq 0.001b$

$$D_i = 9.1098 \sin^2\delta \cos \delta \rho V^2 b^2 \tag{69}$$

Aerodynamic Forces

Solving equation (46) for F_x and substitution into equation (45) gives the lift force,

$$L = F_z \sec \delta - D_i \tan \delta \tag{70}$$

From equation (55), after substituting for Γ_o,

$$F_z = 3.8757 \sin \delta \cos \delta \rho V^2 b^2 \tag{71}$$

From equations (69), (70), and (71), the final expressions for the lift and drag forces are

$$L = \rho V^2 b^2 (3.8757 \sin \delta - 9.1098 \sin^3\delta)$$

$$D_i = \rho V^2 b^2 (9.1098 \sin^2\delta \cos \delta)$$

Since $\frac{b^2}{S_w} = A$, the corresponding coefficients may be expressed as

$$\left.\begin{aligned} C_L &= 2A(3.8757 \sin \delta - 9.1098 \sin^3\delta) \\ D_i &= 2A(9.1098 \sin^2\delta \cos \delta) \end{aligned}\right\} \tag{72}$$

It follows from equations (72) that the forces are directly proportional to the aspect ratio A.

The results of equations (72), obtained by using δ as a parameter, are plotted in figure 23 in the form $\frac{C_L}{A}$ against $\frac{C_{Di}}{A}$. The linearized lifting-line result $\frac{C_L}{A} = \sqrt{\pi \frac{C_{Di}}{A}}$ is included for comparison.

and by using the following integral for the induced drag corresponding to the energy in the region $0.001b \leq r \leq \frac{b}{3}$,

$$\rho \cos \delta \frac{\Gamma_o^2}{4\pi^2} \int_{0.001b}^{b/3} \int_0^{2\pi} \left\{ \left[\frac{r \sin \theta}{\left(\frac{\pi}{4} b + r \cos \theta\right)^2 + (r \sin \theta)^2} - \frac{\sin \theta}{r} \sqrt{1 - \frac{1}{b^2}(b - 3r)^2} \right]^2 + \left[\frac{\frac{\pi}{4} b + r \cos \theta}{\left(\frac{\pi}{4} b + r \cos \theta\right)^2 + (r \sin \theta)^2} - \frac{\cos \theta}{r} \sqrt{1 - \frac{1}{b^2}(b - 3r)^2} \right]^2 \right\} r \, dr \, d\theta$$

This integral may be evaluated numerically for each core yielding the total value (sum of both cores)

$$5.0056 \rho \cos \delta \frac{\Gamma_o^2}{2\pi^2}$$

The integrations were performed by digital computer using Simpson's rule. Evaluation of equation (68) for the region $0 \leq r \leq 0.001b$ over both cores yields for the induced drag

$$\left[\frac{1}{2} (0.0060 - 0.0000045) + \frac{0.000004}{\pi^2} \right] \frac{\rho \cos \delta \Gamma_o^2}{\pi}$$

This subcore value is an extremely small percentage of the total kinetic energy of the cores and an even smaller percentage of the total flow kinetic energy. Hence it is immaterial whether the velocity field of equation (26) or that due to a subcore of constant vorticity (as is the actual case) is used to determine the kinetic energy of the flow near the core center, since the value is in either case negligible. This is true, of course, only if the radius of the constant vorticity subcore is small, and experiment shows this to be the case (ref. 4).

Substitution of the final values for integrals (a) and (b) into equation (57) and replacing Γ_o with $\frac{\pi^2}{2} Vb \sin \delta$ gives the induced drag as a function of δ as follows:

DISCUSSION OF RESULTS

One of the most important results to be noted from the normalized drag polar of figure 23 is that a maximum lift coefficient exists and this maximum coefficient is proportional to the wing aspect ratio. From equations (72), the maximum lift coefficient is

$$C_{L,max} = 1.94A \tag{73}$$

and this occurs for a wake angle $\delta = 22.1^{\circ}$. Thus $C_{L,max}$ is obtained when $\Gamma_o = 1.86Vb$ for an elliptical circulation loading.

The relation for $C_{L,max}$ (eq. (73)) requires some explanation since it predicts unrealistic values of lift coefficient for wings of large aspect ratio. For example, for $A = 15$, $C_{L,max} = 29.1$. It is clear that for wings of large aspect ratio, $C_{L,max}$ is determined by some effect other than the wake induced velocity. For normal wings such as considered herein, $C_{L,max}$ is set by the physical ability of the section to produce circulation. If a Joukowski profile, as obtained by conformal transformation of a circle of radius a is considered, the theory shows that for the section,

$$C_L = 8\pi \frac{a}{c} \sin \alpha_a$$

where c is the chord of the profile and α_a is the absolute angle of attack of the zero lift line. This angle α_a determines the circulation around the section, since the Kutta condition requires that the point on the circle corresponding to the profile trailing edge be a stagnation point. The maximum value of a/c is 1/2, so that for this case

$$C_L = 4\pi \sin \alpha_a$$

and

$$C_{L,max} = 4\pi$$

for $\alpha_a = \frac{\pi}{2}$. When $\alpha_a = \frac{\pi}{2}$, the front and rear stagnation points for both the circle and the profile have coincided. For the profile, both stagnation points then lie on the trailing edge, and any further production of circulation is impossible from a physical standpoint. If all profiles are assumed to behave in a manner similar to the Joukowski

profile, the limit $C_{L,max} = 4\pi = 12.6$ may be set for all profiles. Now assuming that a maximum section lift coefficient of 12.6 can be attained by each section of the three-dimensional wing, the wing lift coefficient cannot exceed 12.6. Hence, regardless of aspect ratio, the absolute $C_{L,max}$ of the wing cannot exceed 12.6. This leads to the conclusion that only wings having $A \leqq 6.5$ will have $C_{L,max}$ limited by wake effects. Here $A = \frac{b^2}{S_w}$ where

$$S_w = \int_{-b/2}^{b/2} c \, dy$$

These results are summarized in figure 24 which is a plot of maximum circulation lift coefficient against aspect ratio. Below an aspect of 6.5 $C_{L,max}$ is given by the relation

$$C_{L,max} = 1.94A$$

Above this value of A, $C_{L,max}$ is equal to 12.6. This curve may be considered the boundary of all possible circulation lift coefficients. (See fig. 24.)

A brief analysis of the physical meaning of C_L/A is of interest. In the derivations only an elliptical distribution of circulation is considered to exist for each value of Γ_o, without regard to the physical means for obtaining such a distribution. In practice any number of wing configurations producing a given lift coefficient and having elliptical circulation can be had merely by a suitable combination of chord, camber, and twist distributions, for the same span. Hence the aspect ratio $A = \frac{b^2}{S_w}$ can scarcely have any unique physical meaning, since it depends upon the particular S_w chosen for its definition. The value of S_w to be used in computing the value of A for use with figure 23 is therefore arbitrary, so long as the same value is used to define the lift coefficient for the wing. This follows from the fact that the normalized lift coefficient is independent of wing area:

$$\frac{C_L}{A} = \frac{L}{qS_w} \frac{S_w}{b^2} = \frac{L}{qb^2}$$

Thus, figure 23 may be used as the drag polar for wings which appreciably alter their geometry and area for various regions of the lift range, provided of course that the circulation distribution at each lift condition approximates the elliptical form. The problem of designing a wing which will possess an elliptical or any other specified distribution of circulation at a given C_L necessitates a knowledge of the downwash distribution at the wing and, as previously mentioned, this information cannot be furnished by momentum considerations.

The Prandtl lifting-line result $\frac{C_L}{A} = \left(\pi \frac{C_{Di}}{A}\right)^{1/2}$ is shown in figure 23 for comparison with equations (72). No appreciable deviation of the linear and nonlinear relations occurs below $\frac{C_L}{A} = 1.1$. Thus use of the linear-theory result $C_{Di} = \frac{C_L^2}{\pi A}$ for calculation of the induced drag appears valid up to the values of lift coefficient equal to the aspect ratio of the wing. This result is also summarized in figure 24 which shows a plot of the equation $C_L = 1.1A$. For combinations of C_L and A below this line, lifting-line theory is valid. Above this line the nonlinear relation of equations (72) is applicable.

Unfortunately, experimental data at sufficiently high values of C_L/A for comparison with the nonlinear region of the theoretical results do not exist. However considerable data are available for boundary-layer-control wings of various aspect ratios and planforms operating at moderate values of C_L, and experimental results (refs. 5 to 13) for several wings are compared with the theory in figure 25. As shown in the figure, the experimental points represent a range of aspect ratios, planforms, and boundary-layer-control systems. In all cases the maximum lift coefficient of the wing is limited by stall, and the points shown represent values just before the stall of the wing. The data correlate well with the normalized polar, even for the rectangular planform and wing-body configurations. The data for the wing of aspect ratio 20 correlate especially well, as might be expected. Reasonable agreement occurs even for wings with appreciable amounts of sweepback. This agreement may be considered as experimental verification of the theoretical prediction that the lifting-line relations are valid even for high lift coefficients provided the aspect ratio is sufficiently large $\left(C_L \leqq 1.1A\right)$.

An additional point of interest in figure 23 is the relation $C_L = C_{Di}$. At $\frac{C_L}{A} = 1.90$, $\frac{C_L}{A} = \frac{C_{Di}}{A}$, and if the total drag of the wing

is assumed to equal the induced drag the thrust required for flight is equal to the lift. Thus, an aircraft capable of operating at $C_L \geq 1.90A$ must have sufficient thrust to take off vertically. This result may be used as a rough demarcation line between STOL and VTOL capabilities of a given STOL aircraft.

The drag polar of figure 23 as established by this investigation is similar to that arrived at by Helmbold (ref. 14) using a different procedure. The agreement is due, however, to the fact that the axial velocity field is assumed negligible in the present treatment. In the derivations of reference 14, no restrictions were placed on the induced axial velocity so that the agreement with the present results indicates that the assumptions of reference 14 reduce it to a two-dimensional treatment of the problem.

The result given in equation (42) predicting downstream distance at which the vortex sheet is fully rolled up may be compared with the result of Kaden (ref. 2). Kaden's relation for an elliptical sheet,

$$d = 0.28b \frac{A}{C_L}$$

may be put in the form

$$\frac{d}{b} = 0.04 \cot \delta$$

for small values of δ, since $\frac{C_L}{A} = \frac{\pi}{2} \frac{\Gamma_o}{Vb}$. From equation (42),

$$\frac{d}{b} = 0.12 \cot \delta$$

The present theory predicts a distance three times as large as does Kaden's result. However, Kaden's derivation is based upon the rollup of a semi-infinite vortex sheet, so that the question as to when the rollup is complete is indeterminate, making the coefficient 0.28 somewhat arbitrary in nature. The result of the present theory is based on complete rollup of a finite semisheet. The apparent difference in the two results is practically negligible, however, as may be seen by a consideration of figure 9. Here it is seen that the greater part of the vorticity is concentrated near the center of the core so that, for example, when the core has grown to only 64 percent of its final radius $\left(\frac{2r}{b} = 0.44\right)$ it already contains 92 percent of the vorticity. Using this radius, $r = 0.22b$ (where equations (20) and (22) diverge

appreciably), as the basis for essentially complete rollup, the result from equation (40) is

$$\frac{d}{b} = 0.05 \cot \delta$$

which may be taken as the "essentially" complete rollup distance. This choice of radius is, however, purely arbitrary and the complete rollup distance is given by

$$\frac{d}{b} = 0.12 \cot \delta$$

That the complete rollup requires considerably more distance than the essentially complete rollup is shown in the experimental data of Muttray (fig. 18 of ref. 15) where the vortex cores move inward laterally toward the equilibrium line $y = \frac{\pi}{8} b$ only very slowly.

A knowledge of the rollup distance is primarily of interest in estimating the downwash field for longitudinal stability analyses. In lieu of accurate experimental data, a first-order approximation of the downwash field behind a highly loaded wing might be estimated from the foregoing results. For this purpose the relation $\frac{d}{b} = 0.05 \cot \delta$ is plotted in figure 26 as a function of C_L/A by using equations (68). This plot shows for example, that the vortex sheet of a wing with aspect ratio 6 pulling a lift coefficient of 3 $\left(\frac{C_L}{A} = 0.5\right)$ will be essentially rolled up at a distance $d = 0.76b$ along the wake axis. If the tail location is such that it lies beyond d for a given C_L/A, the velocity field may be estimated by use of equations (58) and (67). If the tail is located forward of d the velocity field might be roughly estimated by use of Kaden's results (ref. 2) for the lateral location of the cores, combined with equation (40) which determines the size of the cores. It is emphasized that this method is quite approximate, but it furnishes a means for first-order analysis of stability effects at high lift coefficients.

CONCLUDING REMARKS

The objective of this paper has been the development of the complete drag polar for wings having an elliptical distribution of circulation and the objective has been sought through a detailed consideration of the wake produced. In the course of the derivations the

assumption was made that the axial velocity within the cores was negligible in its effect on the wing forces and an attempt was made to justify this from both theoretical and experimental considerations. In view of the other simplifying assumptions made in the derivations a more detailed analysis of the axial velocity field does not appear justified.

The resulting theory predicts that the wake induced velocity limits the maximum lift coefficient to a value equal to 1.94 times the wing aspect ratio A for wings with $A \leq 6.5$ and that airfoil section characteristics limit the lift coefficient to 12.6 for wings with $A > 6.5$. The theory also indicates that up to lift-coefficient values of $1.1A$ the results of the linear lifting-line theory are valid. Although experimental data for values of lift coefficient C_L sufficiently high to compare with the theory near $\left(\frac{C_L}{A}\right)_{max}$ are not available, existing data for many current wing planforms using boundary-layer control correlate well with the theoretical results in the lower range of C_L/A. Experimental data indicate that with the relatively small amounts of boundary-layer control currently being used on operational aircraft, the stall lift coefficient is still sufficiently low that linear theory is applicable.

Finally, experimental evidence indicates that the theory predicts with reasonable accuracy the lift-drag relationship near stall $C_{L,max}$ of wings with widely varying planforms, flap deflections, degrees of sweep, and methods of boundary-layer control.

Langley Research Center,
National Aeronautics and Space Administration,
Langley Field, Va., November 14, 1960.

APPENDIX A

THE AXIAL VELOCITY FIELD OF A VORTEX SOLENOID

The vortex lines comprising the vortex sheet which emanates from the trailing edge of a lifting airfoil coil about the tip filament to form concentric helices as they pass downstream. By virtue of their helical form they act as a solenoid, inducing an axial velocity u within the vortex core. The following is a brief derivation of the velocity profile of such a vortex solenoid.

Magnitude of u Due to a Single Vortex Ring of Radius r

Far downstream the solenoid can be considered as having infinite length and being circular in form. The number of turns per unit length of each helix is assumed sufficient that each turn can be considered to lie in a plane normal to the axis. From induction theory, the axial velocity induced at its center by a ring of radius r is

$$\Delta u_{center} = \frac{d\Gamma}{4\pi r^2} \int_0^{2\pi} r \, d\theta = \frac{d\Gamma}{2r} \tag{A1}$$

where $d\Gamma$ is the strength of the vortex filament and θ is the angle as shown in figure 27. For any point P on the axis of the helix, located a distance x from the ring, the axial velocity induced by the ring is

$$\Delta u_{P,axis} = \frac{d\Gamma r}{4\pi\left(x^2 + r^2\right)^{3/2}} \int_0^{2\pi} r \, d\theta = \frac{r^2 d\Gamma}{2\left(x^2 + r^2\right)^{3/2}} \tag{A2}$$

Magnitude of u Due to a Single Infinite Helix of Radius r

If n is the number of turns or vortex rings per unit length of the helix of strength $d\Gamma$ and radius r, then the circulation per unit length is $n \, d\Gamma$. The circulation about a ring of width dx is $n \, d\Gamma \, dx$ (fig. 27). From equation (A2) this ring will induce at a point P on the axis the velocity

$$\Delta u_{P,axis} = \frac{nr^2 d\Gamma \, dx}{2\left(x^2 + r^2\right)^{3/2}} = \frac{nr^2 d\Gamma \, dx}{2R^3}$$

where R is defined in sketch at bottom of figure 27. For the velocity at P due to a length l of the helix (using bottom sketch of fig. 27),

$$\Delta u_{P,axis} = \frac{n\, d\Gamma}{2} \int_{\theta_1}^{\theta_2} \sin\theta\, d\theta = \frac{n\, d\Gamma}{2}(\cos\theta_1 - \cos\theta_2)$$

since

$$\frac{n\, d\Gamma}{2R^3} r^2 dx = \frac{n\, d\Gamma}{2R} \frac{R\, d\theta}{\sin\theta} \sin^2\theta = \frac{n\, d\Gamma}{2} \sin\theta\, d\theta$$

When the helix is infinite, $\theta_1 = \theta_2 = 0$ and

$$\Delta u_P = n\, d\Gamma \tag{A3}$$

Velocity Profile $u(r)$ for Entire Vortex Core

A helix of radius r having $n(r)$ turns per unit length and strength $d\Gamma = \frac{d\Gamma}{dr} dr$ contributes an element of axial velocity of

$$du = n(r)\frac{d\Gamma}{dr} dr$$

at all points on the axis of the helix. Since the helix is infinitely long this velocity is constant over the interior. By summing all the helices comprising the core, the axial velocity profile is

$$u(r) = \lim_{k \to \infty} \sum_{i=1}^{k} \Delta u_i = \int_r^{r_o} n(\eta)\frac{d\Gamma}{d\eta} d\eta \tag{A4}$$

where η is a dummy variable of integration, r_o is the outer radius of the vortex core, and k is an integer.

APPENDIX B

ALTERNATE METHOD FOR CALCULATING F_z

The stable wake far downstream from the wing consists of two vortex cores of diameter $\frac{2}{3}b$ with centers $\frac{\pi}{4}b$ apart moving normal to themselves with a velocity $V \sin \delta$ (fig. 10). The relative closeness of the cores results in the formation of two distinct systems of streamlines relative to the cores, as will be shown. One system is closed - that is, the streamlines form closed curves about the cores - whereas, the other consists of open streamlines - that is, beginning and ending at infinity (fig. 28). The result is that the vortex pair entraps the fluid within the closed system and carries it along in its translation with a velocity $V \sin \delta$. The force exerted by the airfoil to give this mass of air the translational velocity $V \sin \delta$ is clearly the aerodynamic force F_z. This force consists of two parts: that associated with the translational momentum of the closed body of fluid and that necessary to accelerate the body of fluid to the velocity $V \sin \delta$. Determination of the time rate of change of the z-impulse associated with the formation of this wake will, as before, give the force F_z.

The calculation is begun by first determining the boundary of the closed body, that is, the enclosing streamline, from which the sectional area may be established. Since each core has a strength κ_o the complex potential of the steady flow is, in terms of the complex variable $z' = y + iz$,

$$W(z) = \frac{\Gamma_o}{2\pi} i\left[\log_e (z' - z_1') - \log_e (z' - z_2')\right] + (V \sin \delta) e^{i\left(-\frac{\pi}{2}\right)} z' \qquad (B1)$$

whence

$$\psi = \frac{\Gamma_o}{2\pi} \log_e \frac{\left[(y - y_1)^2 + z^2\right]^{1/2}}{\left[(y - y_2)^2 + z^2\right]^{1/2}} - Vy \sin \delta \qquad (B2)$$

Here y and z are Cartesian coordinates. The bounding streamline is given by $\psi = 0$, and since $\Gamma_o = \frac{\pi^2}{2} Vb \sin \delta$, the equation of the boundary becomes, after some transformations,

$$y = \frac{\pi}{8} b \left\{ \log_e \left[\left(y + \frac{\pi}{8} \right)^2 + z^2 \right] - \log_e \left[\left(y - \frac{\pi}{8} \right)^2 + z^2 \right] \right\} \qquad (B3)$$

This implicit equation can be solved graphically to obtain the boundary streamline. The section of the wake is an oval with minor axis of $0.926b$ and major axis of $1.639b$, with an area of $1.760b^2$. As is evident from equation (B3), the cross-sectional area is independent of both Γ_o and core radius.

The wake may thus be considered as a fluid cylinder of oval section moving normal to its axis with velocity of $V \sin \delta$. This cylinder carries a momentum per unit length of

$$\rho A' V \sin \delta \qquad (B4)$$

where $A' = 1.760b^2$, the sectional area of the cylinder. The part of the force F_z due to the cylinder momentum is obtained from the time rate of change of the wake z-momentum due to the creation of the cylinder,

$$(F_z)_1 = \rho V^2 \sin \delta \cos \delta A' = 1.760 \rho V^2 b^2 \sin \delta \cos \delta \qquad (B5)$$

The second part of the force F_z is that associated with the flow momentum external to the cylinder. The fluid motion external to the fluid cylinder is identical to that associated with the motion of a solid cylinder of the same shape. As predicted by hydrodynamic theory, the application of a definite impulse is required to accelerate an immersed body from rest to a steady velocity U in a fluid also at rest initially, and this impulse is greater than that needed for equal acceleration in a vacuum. Thus the presence of the fluid increases the effective mass of the body by an amount M', the hydrodynamic mass, which is equal to the drift mass of the particular body.

The power expended in generating a unit length of the exterior flow about a solid cylinder of any sectional shape moving normal to its axis is

$$\frac{dE}{dt} = F'U = M'U \frac{dU}{dt} \qquad (B6)$$

where F' is the part of the total force which must be applied to the body to overcome its acceleration drag. Converting equation (B6) to an impulse gives

$$\int F'dt = M'U = I' \tag{B7}$$

where I' is the impulse per unit length of cylinder to generate the external motion from rest. The determination of the second part of F_z now reduces to a calculation of M' for the oval cylinder of the wake.

The oval is assumed to be a true ellipse, since it varies only slightly from an ellipse with similar minor and major axes. The kinetic energy in the flow exterior to an elliptical cylinder with major axis $2a$ and minor axis $2b$, moving with the steady velocity U normal to its semiaxis a is, per unit length,

$$E = \frac{1}{2}\rho\pi U^2 a^2 \tag{B8}$$

Using equation (B6) yields

$$M' = \rho\pi a^2 \tag{B9}$$

for the cylinder drift mass. In the present case $a = 0.819b$ and $U = V \sin \delta$, and I' is obtained from equation (B7) as

$$I' = (0.819)^2\rho\pi b^2 V \sin \delta$$

Then

$$(F_z)_2 = \frac{dI}{dt} = 2.116\rho V^2 b^2 \sin \delta \cos \delta$$

Finally,

$$F_z = (F_z)_1 + (F_z)_2 = 3.876\rho V^2 b^2 \sin \delta \cos \delta \tag{B10}$$

These results indicate that the fluid within the closed body carries 45.4 and the external flow 54.6 percent of the z-momentum imparted by the airfoil to the fluid.

It is of interest to compare these results with those of the usual momentum treatment of airfoil lift, wherein it is represented that the airfoil obtains lift by imparting a downward velocity $\bar{w} = \frac{\Gamma_o}{b}$ to a mass of air passing through a circle of diameter equal to the wing span

$$L = \rho \frac{\pi b^2}{4} \frac{\Gamma_o}{b} V \cos \delta$$

For small values of δ ($\cos \delta \rightarrow 1$), this expression reduces to

$$L = \frac{\pi^3}{8} \rho V^2 b^2 \sin \delta$$

so that

$$L = 3.876 \rho V^2 b^2 \sin \delta$$

This is identical with the previous result for F_z. However, the present treatment gives the true physical wake, while the circular form has no physical reality.

REFERENCES

1. Betz, A.: Behavior of Vortex Systems. NACA TM 713, 1933.

2. Kaden, H.: Aufwicklung einer unstabilen Unstetigkeitsfläche. Ing.-Archiv, Bd. II, Heft 2, May 1931, pp. 140-168.

3. Westwater, F. L.: Rolling Up of the Surface of Discontinuity Behind an Aerofoil of Finite Span. R. & M. No. 1692, British A.R.C., 1935.

4. Fage, A., and Simmons, L. F. S.: An Investigation of the Air-Flow Pattern in the Wake of an Airfoil of Finite Span. R. & M. No. 951, British A.R.C., 1926.

5. Croom, Delwin R., and Turner, Thomas R.: Low-Speed Boundary-Layer-Control Investigation on a Thin Rectangular Semispan Wing With Leading-Edge and Trailing-Edge Flaps. NACA RM L57J15, 1958.

6. Holzhauser, Curt A.: Wind-Tunnel Investigation of the Use of Leading-Edge and Trailing-Edge Area-Suction Flaps on a 13-Percent-Thick Straight Wing and Fuselage Model. NACA RM A57K01. 1958.

7. Kelly, Mark W., and Tolhurst, William H., Jr.: The Use of Area Suction to Increase the Effectiveness of a Trailing-Edge Flap on a Triangular Wing of Aspect Ratio 2. NACA RM A54A25, 1954.

8. Griffin, Roy N., Jr., and Hickey, David H.: Investigation of the Use of Area Suction to Increase the Effectiveness of Trailing-Edge Flaps of Various Spans on a Wing of 45° Sweepback and Aspect Ratio 6. NACA RM A56B27, 1956.

9. Holzhauser, Curt A., Martin, Robert K., and Page, V. Robert: Application of Area Suction to Leading-Edge and Trailing-Edge Flaps on a 44° Swept-Wing Model. NACA RM A56F01, 1956.

10. Koenig, David G., and Aoyagi, Kiyoshi: The Use of a Leading-Edge Area-Suction Flap and Leading-Edge Modifications to Improve the High-Lift Characteristics of an Airplane Model With a Wing of 45° Sweep and Aspect Ratio 2.8. NACA RM A57H21, 1957.

11. Cocke, Bennie W., Jr., Fink, Marvin P., and Gottlieb, Stanley M.: The Aerodynamic Characteristics of an Aspect-Ratio-20 Wing Having Thick Airfoil Sections and Employing Boundary-Layer Control by Suction. NACA TN 2980, 1953.

12. Holzhauser, Curt A., and Martin Robert K.: The Use of a Leading-Edge Area-Suction Flap to Delay Separation of Air Flow From the Leading Edge of a 35° Sweptback Wing. NACA RM A53J26, 1953.

13. Holzhauser, Curt A., and Bray, Richard S.: Wind-Tunnel and Flight Investigations of the Use of Leading-Edge Area Suction for the Purpose of Increasing the Maximum Lift Coefficient of a 35° Swept-Wing Airplane. NACA Rep. 1276, 1956. (Supersedes NACA RM A52G17 by Holzhauser and Martin and RM A55C07 by Bray and Innis.)

14. Helmbold, H. B.: Theory of the Highly Loaded Finite Span Wing. Rep. No. RR-35, Fairchild Aircraft (Hagerstown, Md.), Sept. 26, 1956.

15. Muttray, H.: Investigations on the Amount of Downwash Behind Rectangular and Elliptical Wings. NACA TM 787, 1936.

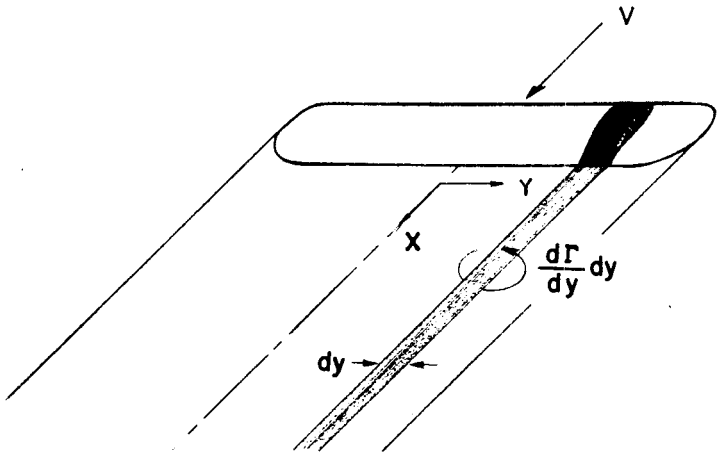

Figure 1.- Trailing vortex system behind a finite-span wing.

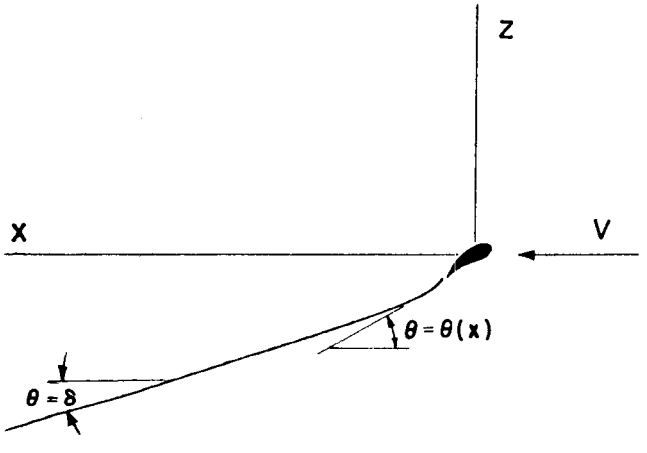

Figure 2.- General representation of the vortex-wake inclination.

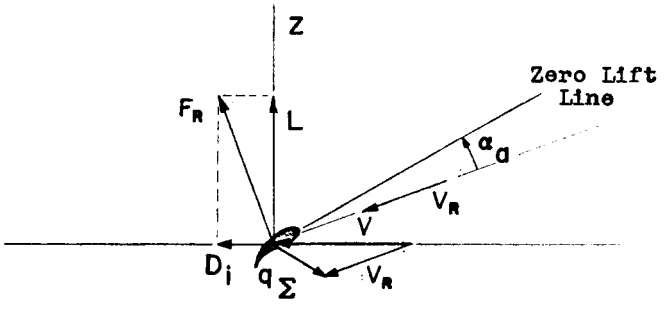

Figure 3.- Forces and velocities acting at a section of a finite-span wing having high circulation.

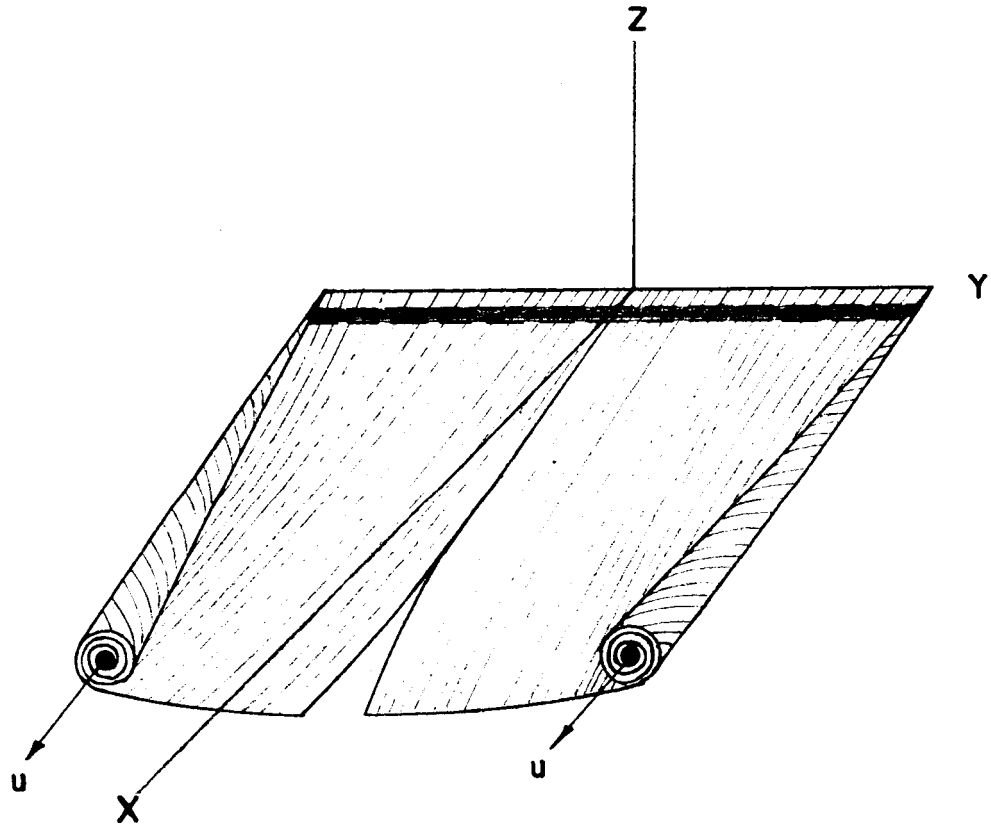

Figure 4.- General representation of the deformation of the trailing vortex sheet behind a finite-span wing.

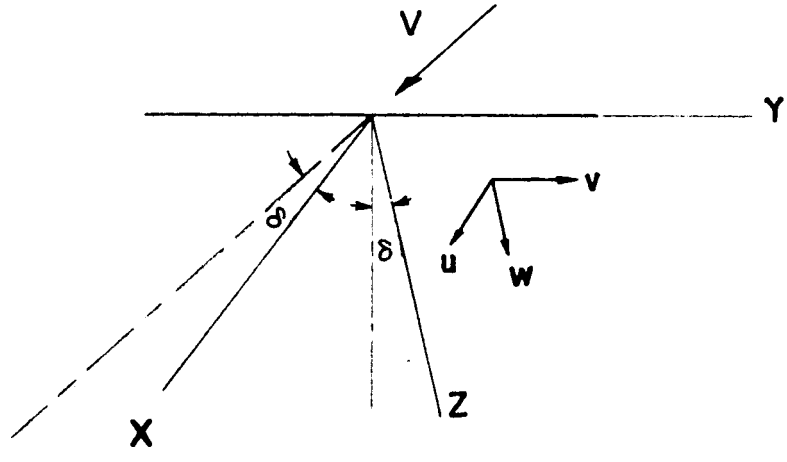

Figure 5.- System of coordinate axes taken parallel to the ultimate wake.

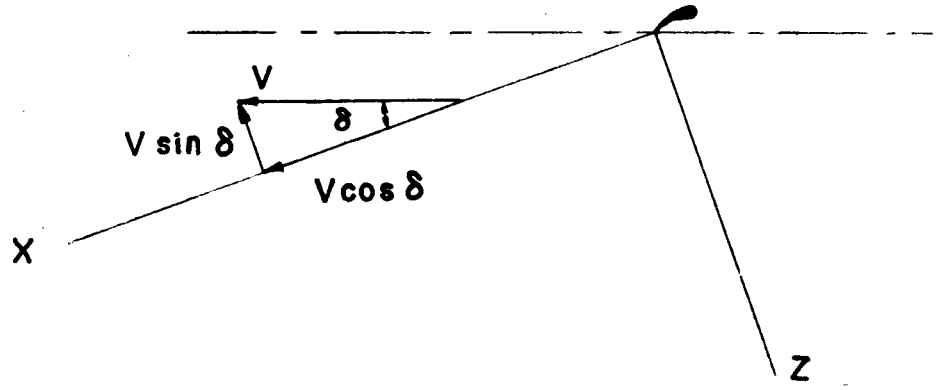

Figure 6.- Components of the free-stream velocity.

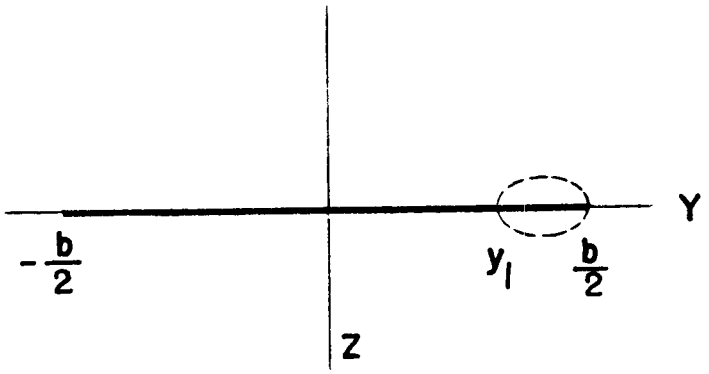

Figure 7.- Axis system for the initially flat wake strip.

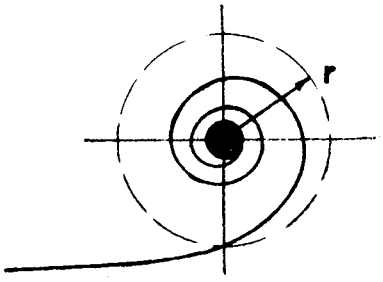

Figure 8.- Coiling vortex sheet. (See ref. 2.)

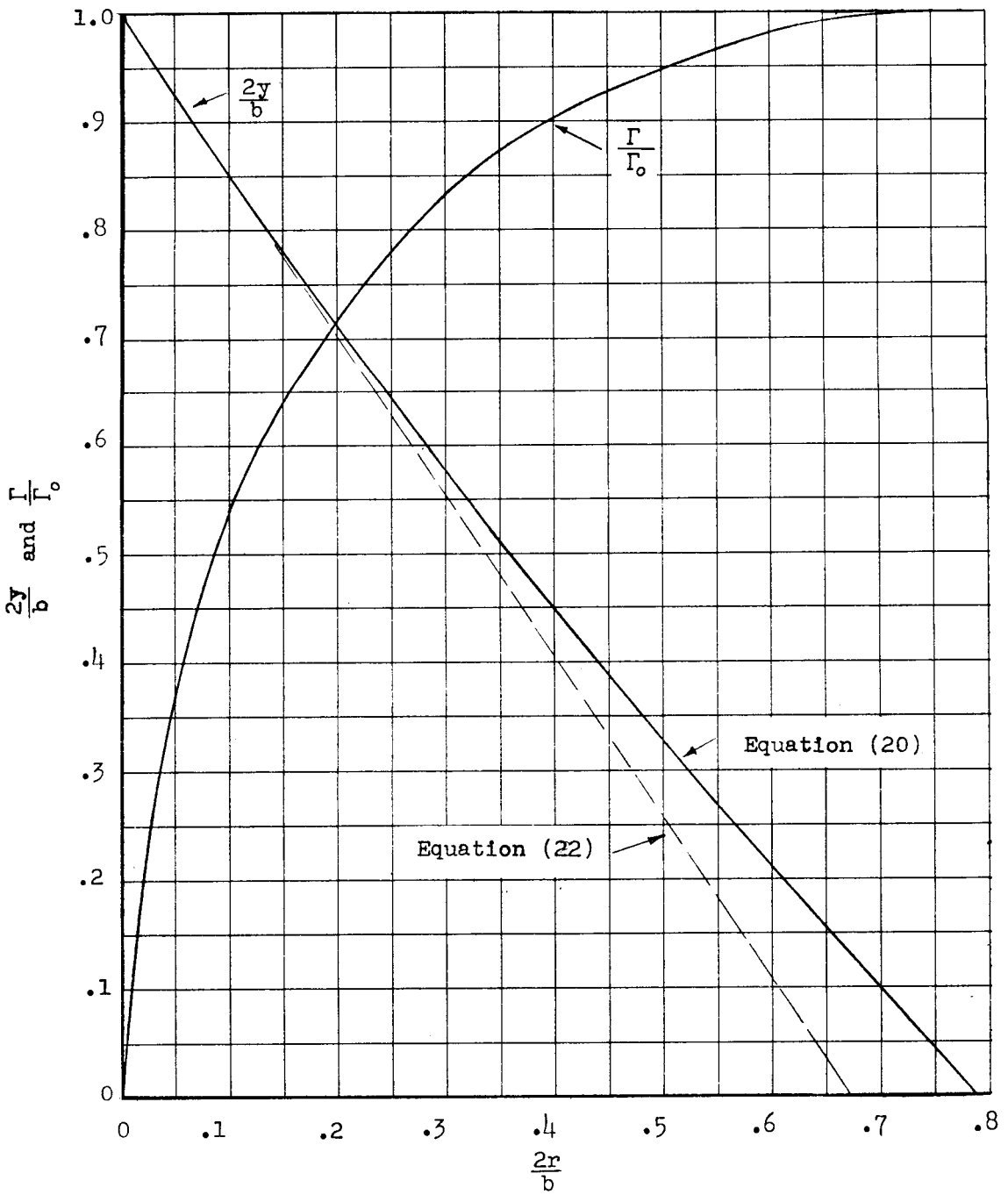

Figure 9.- Variation of circulation with radius and the relation of the vortex sheet to the core size.

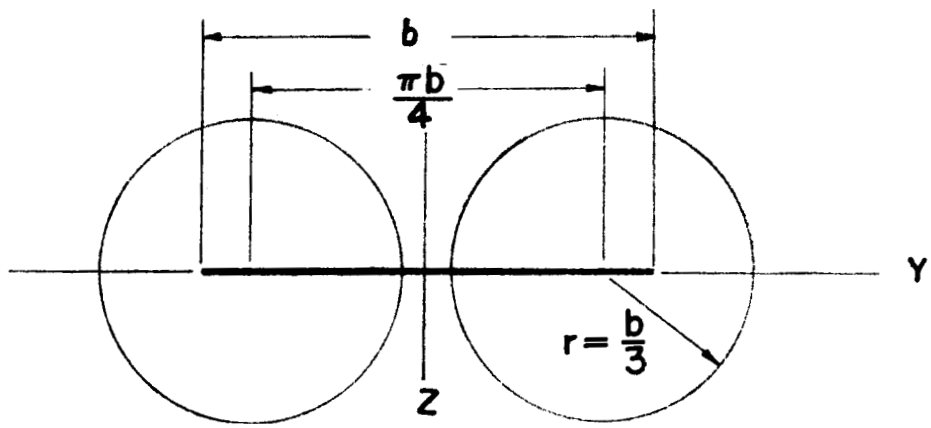

Figure 10.- Cross-sectional view of the ultimate wake taken normal to the core axes.

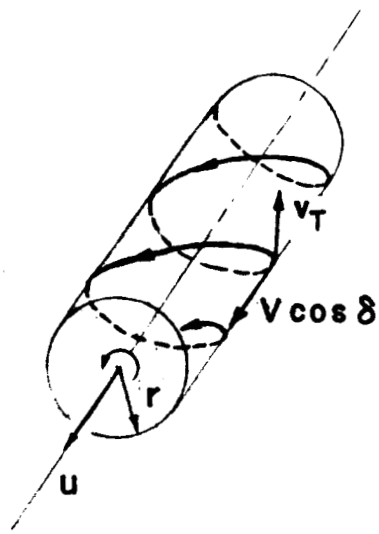

Figure 11.- Elemental length of a vortex helix of radius r formed by the deformation of a vortex sheet wake.

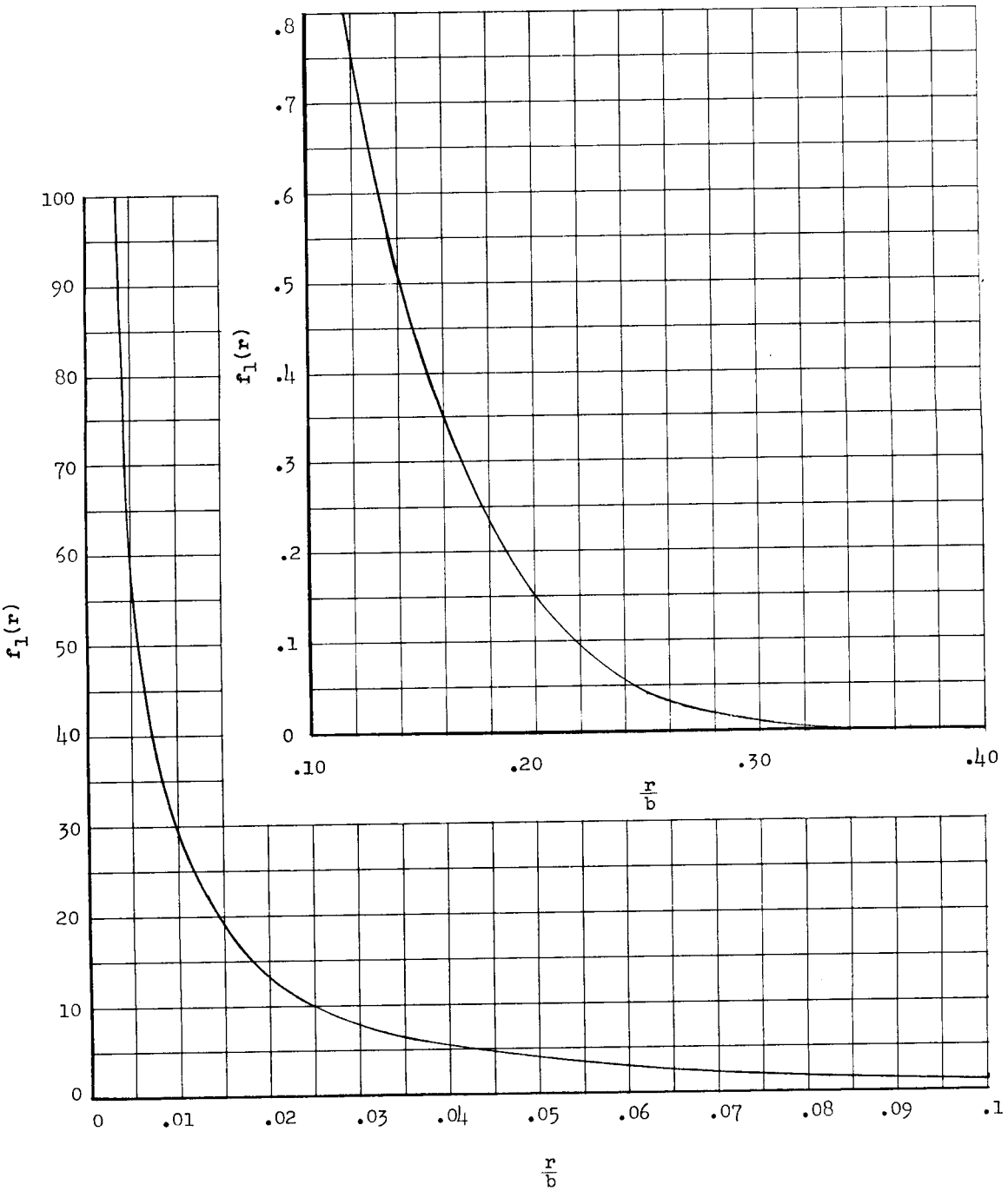

Figure 12.- Variation of the function $f_1(r)$ with radius in the vortex core.

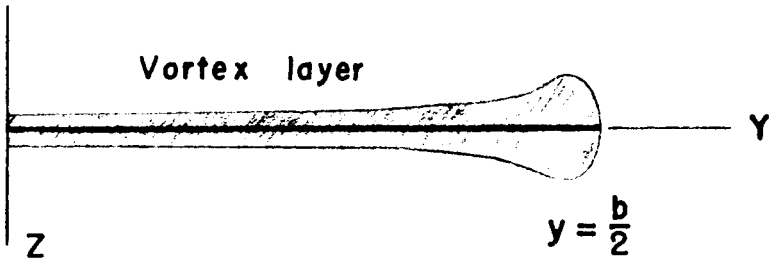

Figure 13.- General representation of the thickness variation of the vortex layer behind a finite-span wing. (See ref. 4.)

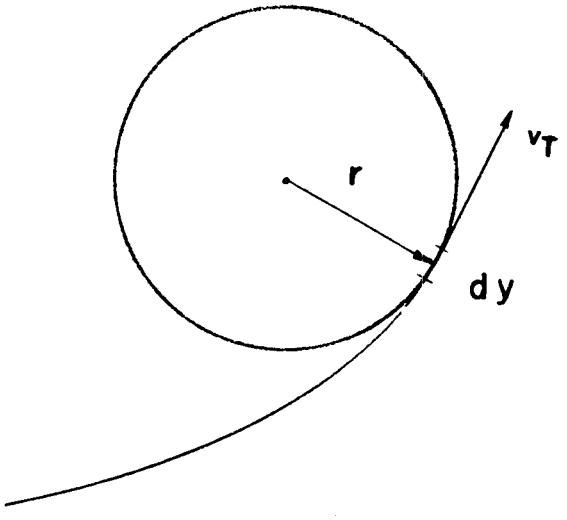

Figure 14.- Addition of the vortex sheet to the vortex core.

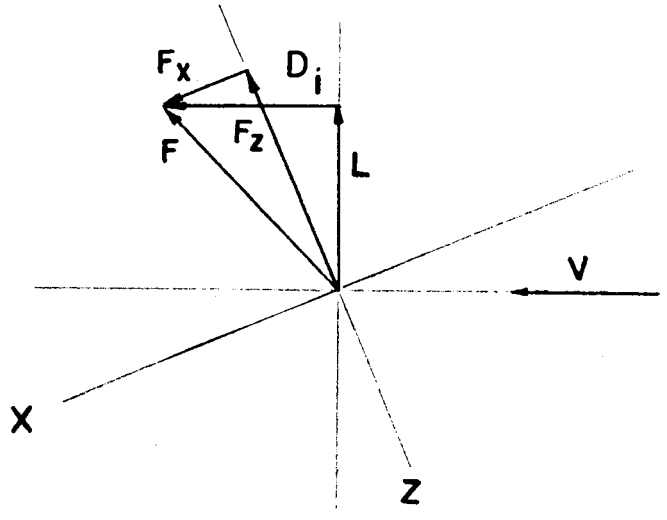

Figure 15.- Force systems for a lifting airfoil.

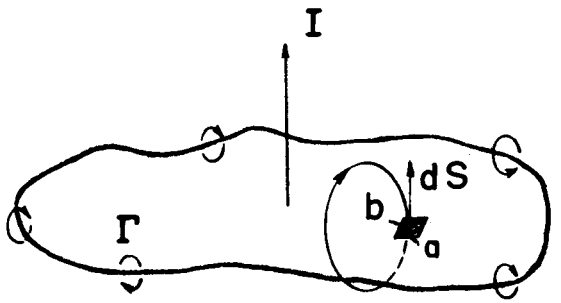

Figure 16.- Impulse surface of a closed vortex filament.

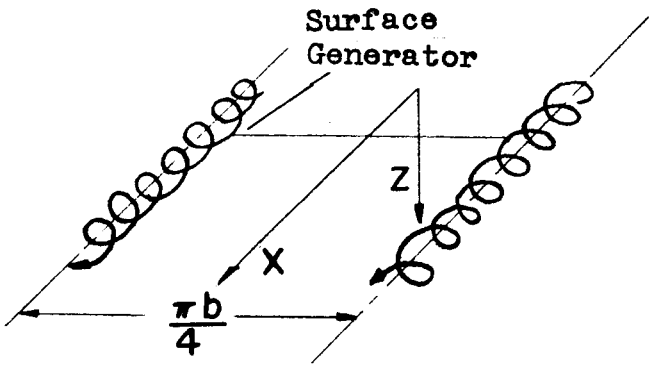

Figure 17.- View of a pair of corresponding vortex helices.

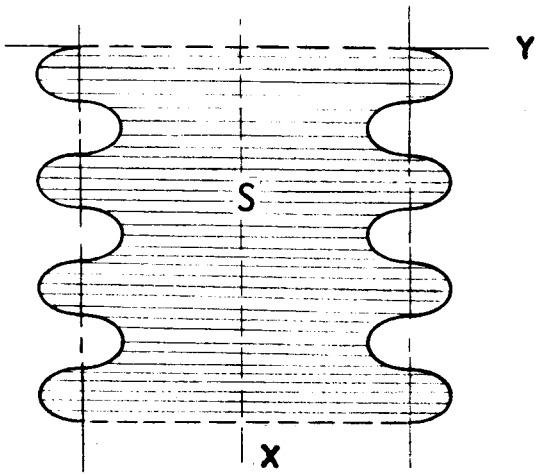

Figure 18.- Impulse surface of a pair of corresponding vortex helices (top view).

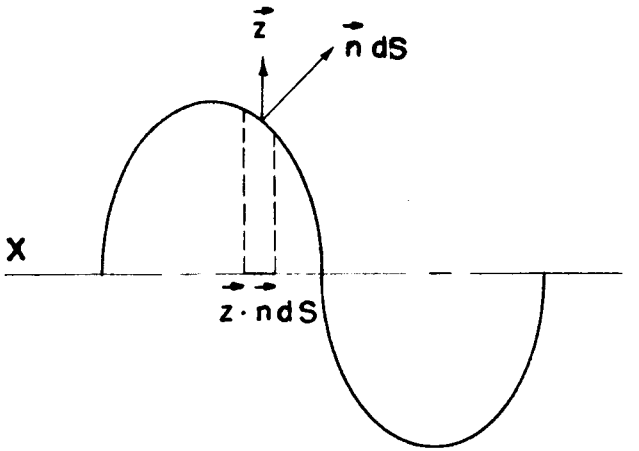

Figure 19.- Impulse surface of a vortex helix (side view).

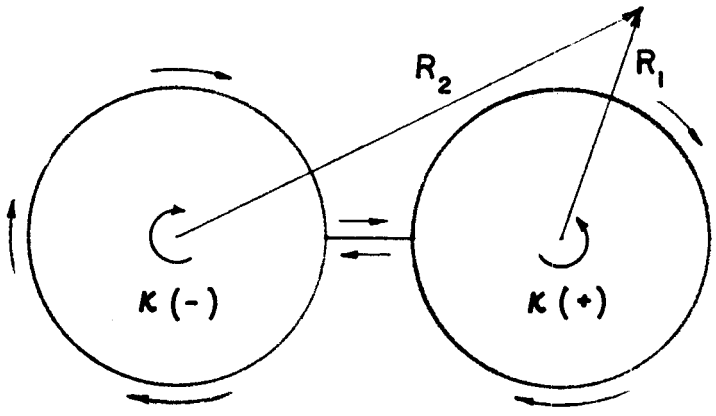

Figure 20.- Path of integration for determining kinetic energy external to a vortex pair.

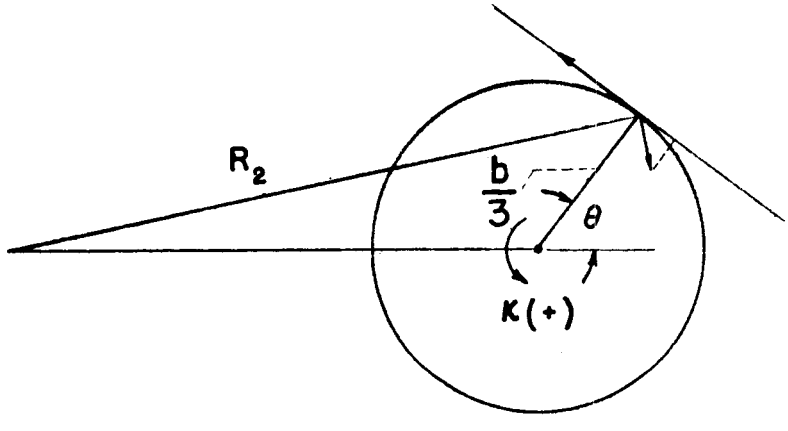

Figure 21.- Geometrical relations for establishing equations (64).

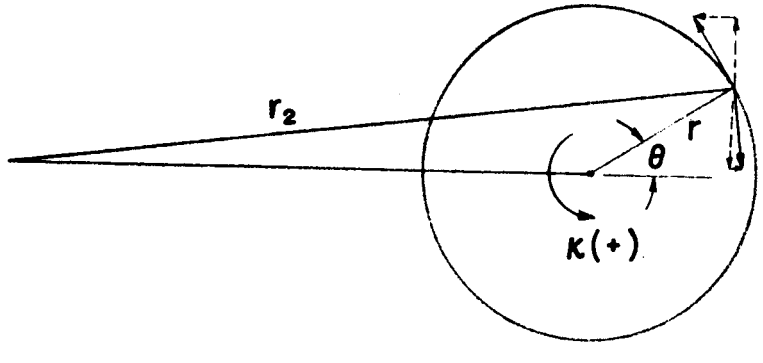

Figure 22.- Geometrical relations for establishing equations (67).

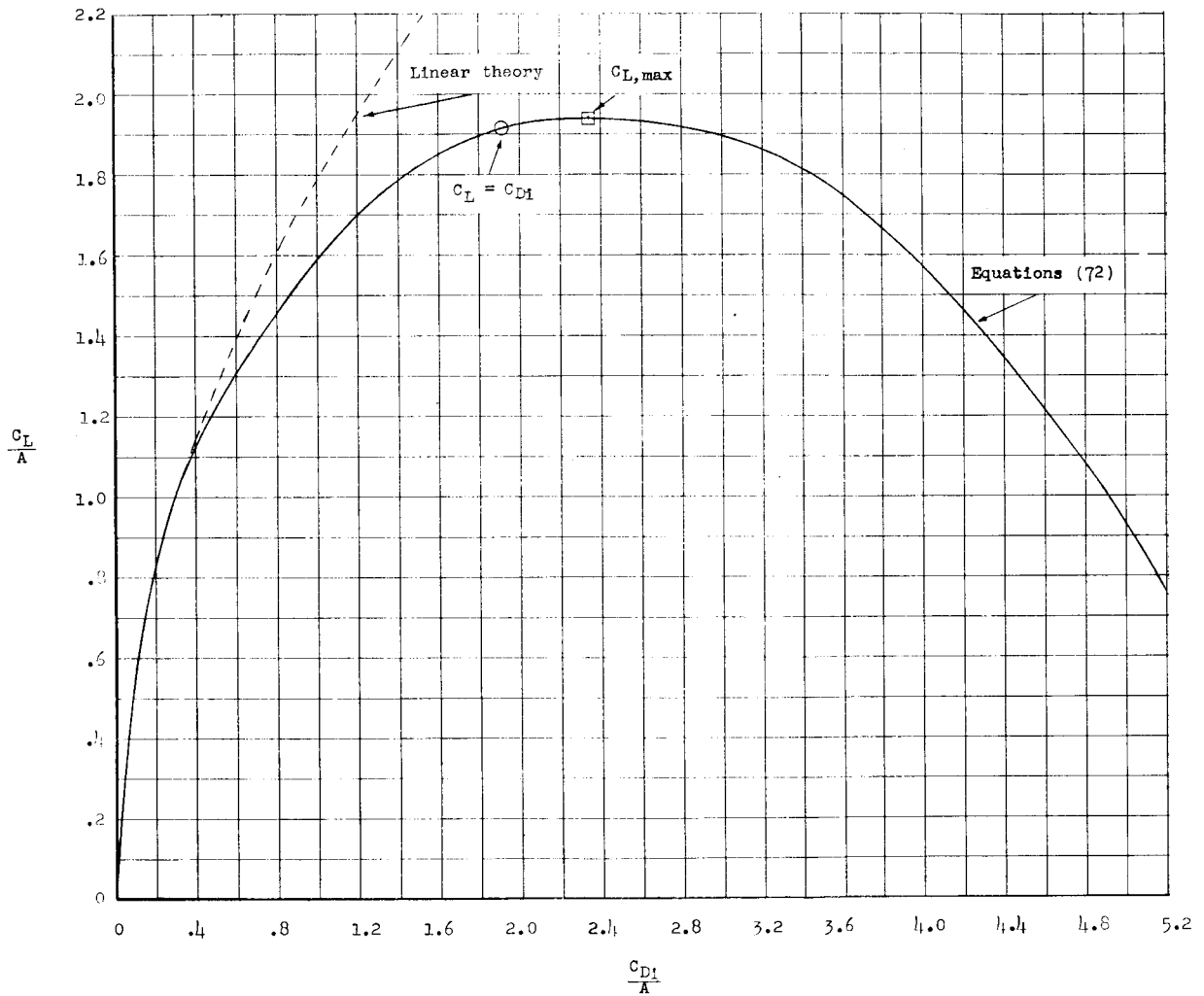

Figure 23.- Complete induced drag polar for finite-aspect-ratio wings having elliptical circulation distribution

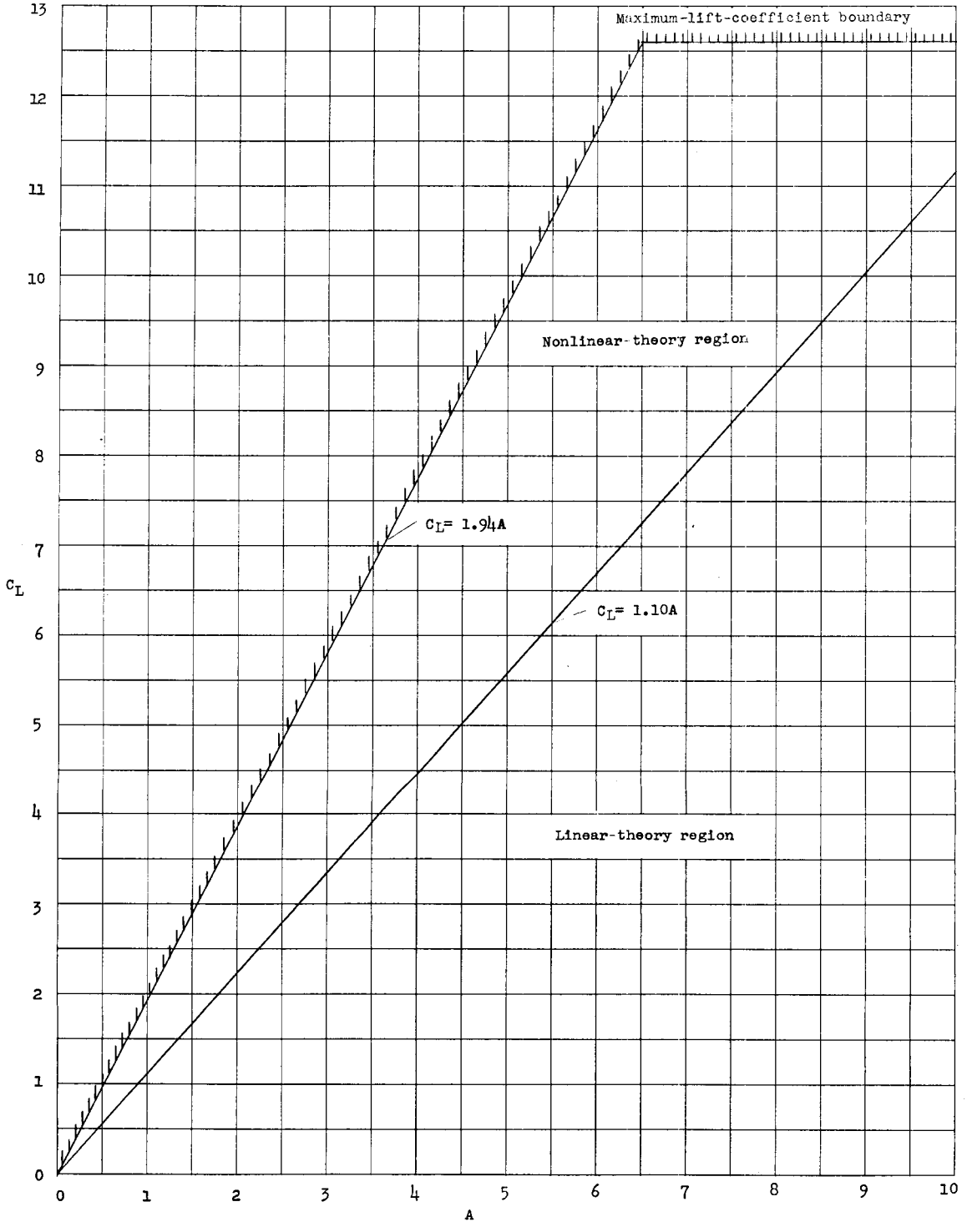

Figure 24.- Variation of lift coefficient with aspect ratio and regions in which linear and nonlinear theory apply for calculation of induced drag.

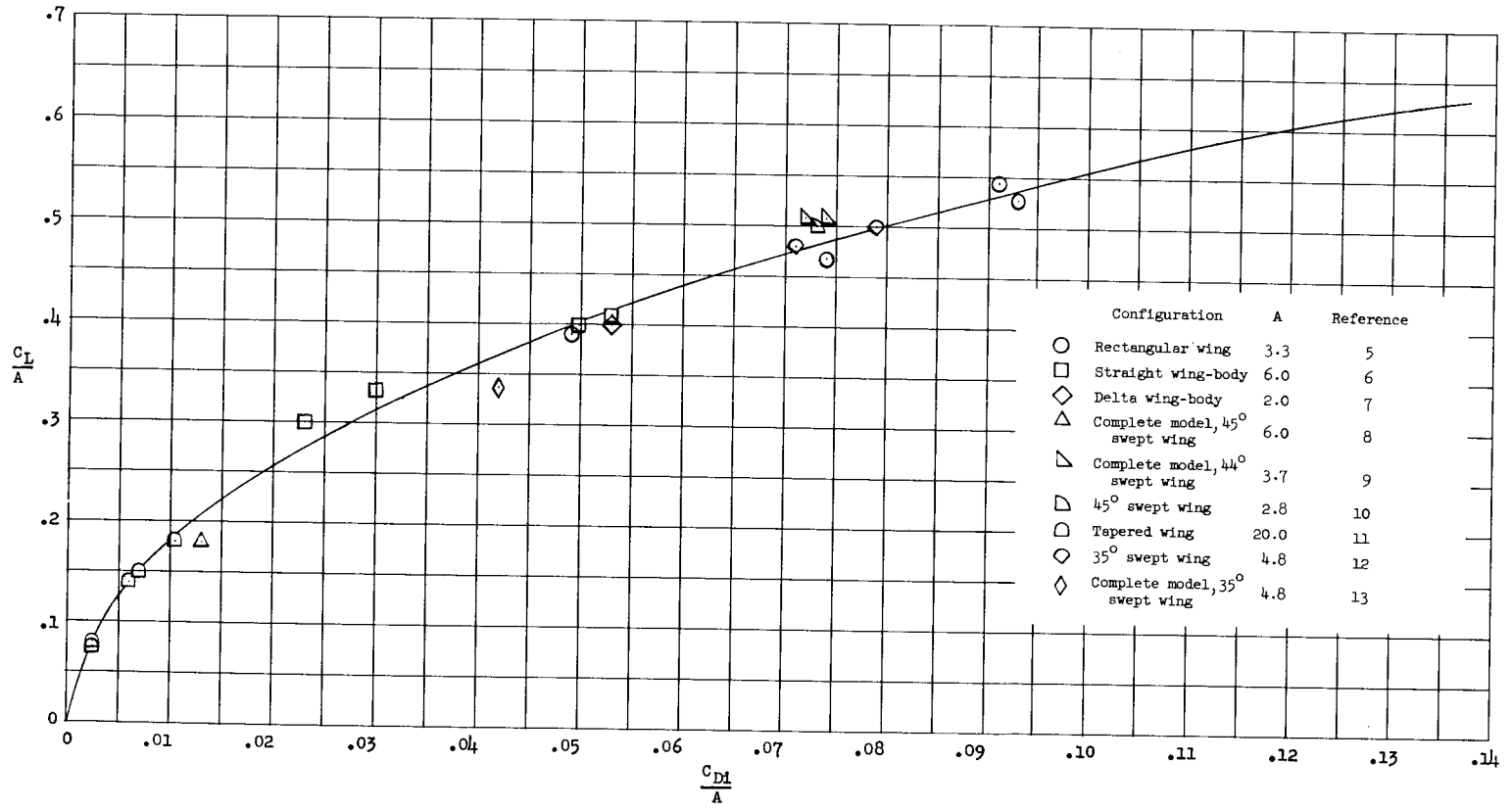

Figure 25.- Comparison of theoretical results with experimental data for various combinations of planform and aspect ratio.

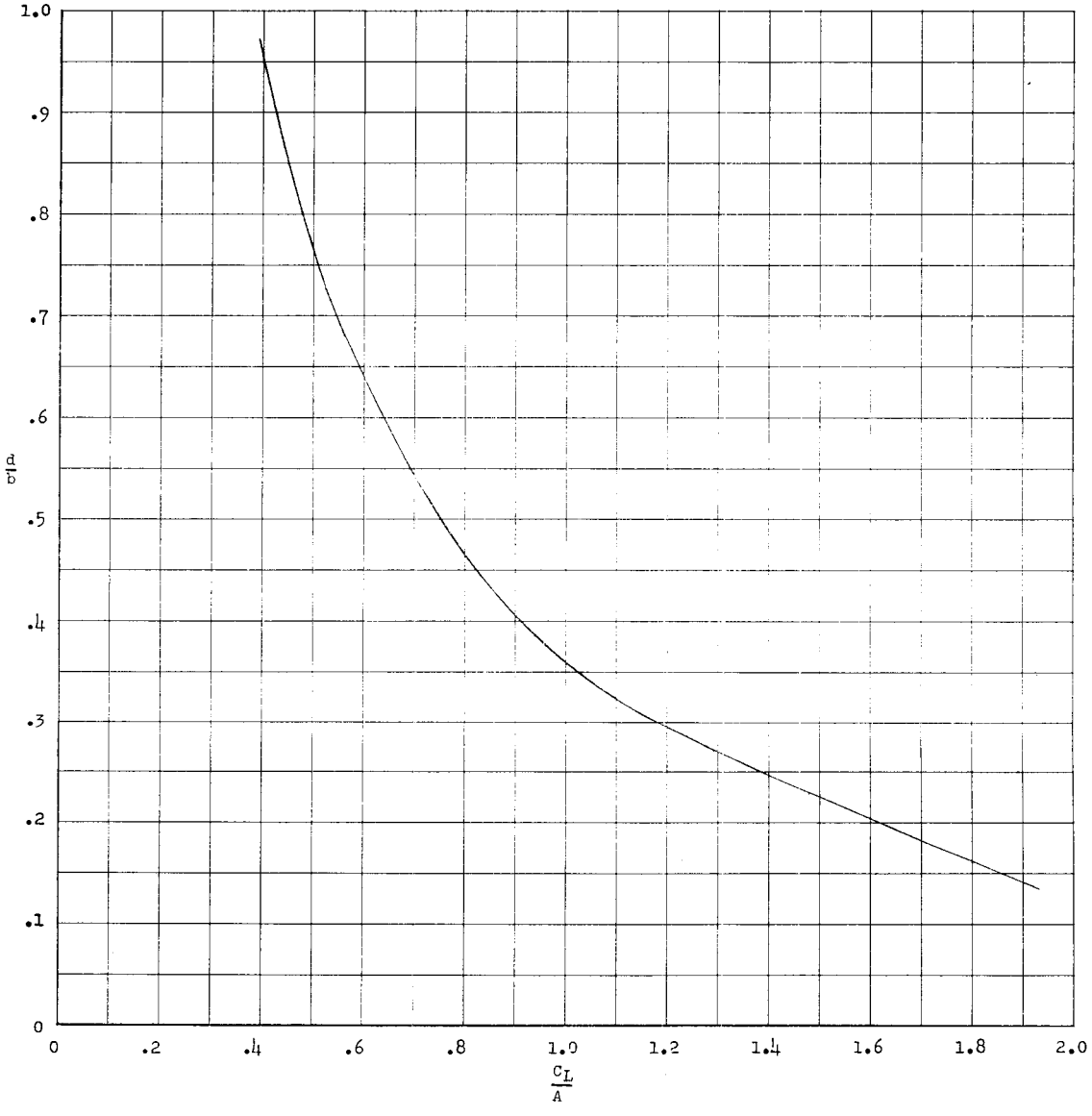

Figure 26.- Relation of rollup distance with normalized lift coefficient.

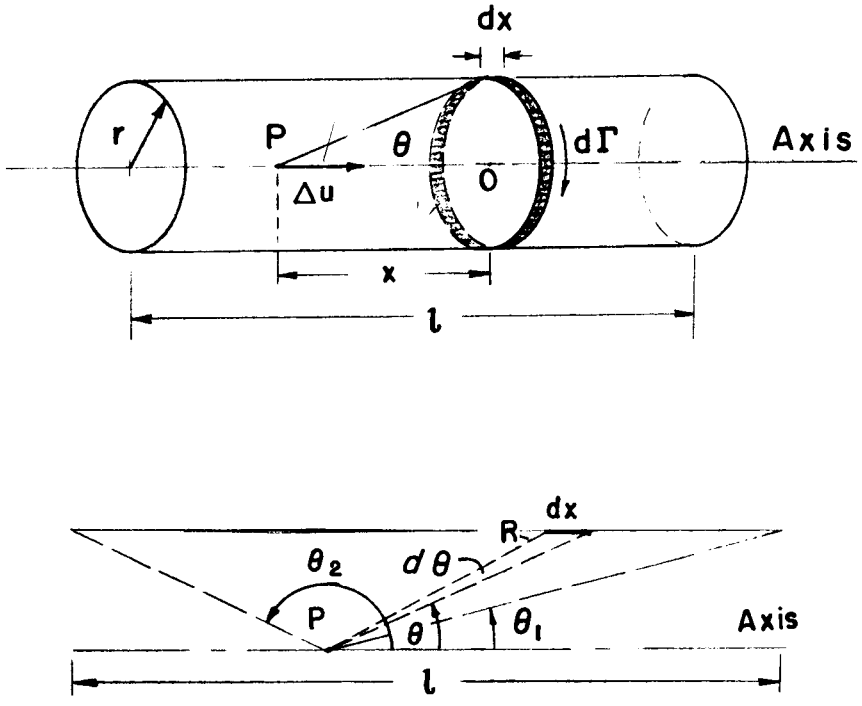

Figure 27.- Geometrical relations for axial-induced velocity field of a vortex helix.

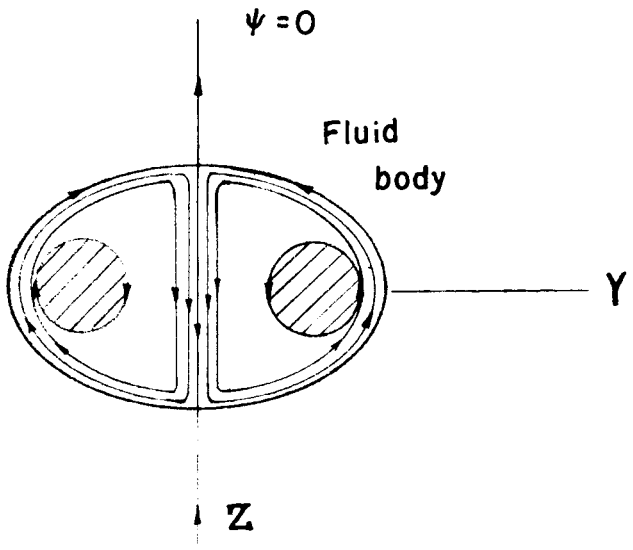

Figure 28.- The streamline $\psi = 0$ which forms the boundary between the open and closed streamline systems.